

# Modeling the cosmological co-evolution of supermassive black holes and galaxies: II. The clustering of quasars and their dark environment

Silvia Bonoli<sup>1\*</sup>, Federico Marulli<sup>2</sup>, Volker Springel<sup>1</sup>, Simon D.M. White<sup>1</sup>, Enzo Branchini<sup>3</sup>, Lauro Moscardini<sup>2,4</sup>

<sup>1</sup>Max-Planck-Institut für Astrophysik, Karl-Schwarzschild Strasse 1, D-85740 Garching, Germany

<sup>2</sup>Dipartimento di Astronomia, Università degli Studi di Bologna, via Ranzani 1, I-40127 Bologna, Italy

<sup>3</sup>Dipartimento di Fisica, Università degli Studi “Roma Tre”, via della Vasca Navale 84, I-00146 Roma, Italy

<sup>4</sup>INFN, Sezione di Bologna, viale Berti Pichat 6/2, I-40127 Bologna, Italy

12 February 2022

## ABSTRACT

We use semi-analytic modeling on top of the Millennium simulation to study the joint formation of galaxies and their embedded supermassive black holes. Our goal is to test scenarios in which black hole accretion and quasar activity are triggered by galaxy mergers, and to constrain different models for the lightcurves associated with individual quasar events. In the present work we focus on studying the spatial distribution of simulated quasars. At all luminosities, we find that the simulated quasar two-point correlation function is fit well by a single power-law in the range  $0.5 \lesssim r \lesssim 20 h^{-1} \text{Mpc}$ , but its normalization is a strong function of redshift. When we select only quasars with luminosities within the range typically accessible by today’s quasar surveys, their clustering strength depends only weakly on luminosity, in agreement with observations. This holds independently of the assumed lightcurve model, since bright quasars are black holes accreting close to the Eddington limit, and are hosted by dark matter haloes with a narrow mass range of a few  $10^{12} h^{-1} M_{\odot}$ . Therefore the clustering of bright quasars cannot be used to disentangle lightcurve models, but such a discrimination would become possible if the observational samples can be pushed to significantly fainter limits. Overall, our clustering results for the simulated quasar population agree rather well with observations, lending support to the conjecture that galaxy mergers could be the main physical process responsible for triggering black hole accretion and quasar activity.

**Key words:** galaxies: active - galaxies: formation - quasars: general - cosmology: observations - cosmology: theory

## 1 INTRODUCTION

At the beginning of this century, very bright quasars powered by black holes (BHs) with masses of the order of  $10^9 M_{\odot}$  were discovered at redshifts up to  $z \sim 6$  (Fan et al. 2000, 2001). At the same time, X-ray observations showed that the space density of Active Galactic Nuclei (AGN) peaks at  $z \sim 2 - 3$ , and AGN with high X-ray luminosities are more common at higher redshift with respect to their low-luminosity counterpart (Steffen et al. 2003; Cowie et al. 2003; Cattaneo & Bernardi 2003; Ueda et al. 2003; Hasinger et al. 2005). Heckman et al. (2004), using optical data from SDSS, found that at low redshift only BHs with a mass  $\lesssim 10^7 M_{\odot}$  are actively growing. Combined, these observations suggest that supermassive black holes (SMBHs) grow “anti-hierarchically”: the more massive

BHs were already in place at high redshift, and since then the accretion activity has shifted to smaller scales.

Understanding how this evolution of BH growth relates to cosmic structure formation, how BH accretion depends on the environment, and how BHs interact with their host galaxies, have become central questions of cosmology that need to be answered for a full understanding of galaxy formation. In fact, it has become clear in recent years that BHs and galaxies are linked and mutually influence each other. This co-evolution has been explored in recent years through analytic, semi-analytic and fully numerical approaches in numerous studies (e.g., Silk & Rees 1998; Kauffmann & Haehnelt 2000; Merloni et al. 2004; Di Matteo et al. 2005; Cattaneo et al. 2005; Croton et al. 2006; Monaco et al. 2007; Malbon et al. 2007; Marulli et al. 2006, 2007).

Starting from Soltan (1982), many papers have combined the present-day BH mass function with the AGN luminosity density of

\* E-mail: bonoli@mpa-garching.mpg.de

quasars at various redshifts to conclude that most of the mass in today's BHs must have been accumulated during phases of bright AGN activity (see also Yu & Tremaine 2002; Elvis et al. 2002; Marconi et al. 2004; Merloni & Heinz 2008). The duration of these highly-efficient accretion phases could range from a few  $10^7$  yr (Yu & Tremaine 2002) up to  $10^8$  yr (Marconi et al. 2004), values that strongly depend on the BH mass range considered and on the assumed radiation efficiency  $\epsilon$ . In fact, the precise value of this quasar lifetime is still an open question (Martini 2004). Estimates of the duration of individual accretion events using, for example, the *proximity effect* (Carswell et al. 1982; Bajtlik et al. 1988), have suggested lifetimes of the order of 1 Myr (Kirkman & Tytler 2008).

Haiman & Hui (2001) and Martini & Weinberg (2001) suggested to use quasar clustering to obtain estimates of the quasar lifetime (see also the seminal work of Cole & Kaiser 1989). The reasoning behind this conjecture is simple: if quasars are strongly clustered, their hosts must be rare objects, and therefore they must also be long events in order to account for the total quasar luminosity density observed. If, on the other hand, their clustering is comparable to the clustering of small dark matter haloes, their hosts must be much more common, and their luminous phases must therefore have short duration.

The advent of wide-field surveys like SDSS and 2dF quasi-stellar object (2dFQSO) (York et al. 2000; Croom et al. 2004) with their observation of thousands of quasars has allowed a detailed investigation of the clustering properties of accreting BHs. Croom et al. (2005) and Porciani et al. (2004) calculated the correlation function of quasars observed in 2dF in the redshift range  $0.5 \lesssim z \lesssim 2$ . Both groups found that the clustering strength is an increasing function of redshift, but that it does not depend significantly on quasar luminosity. The inferred values of the bias would suggest that quasars of the observed luminosities are hosted by haloes of a few  $10^{12} h^{-1} M_{\odot}$ , which remains approximately constant with redshift, since haloes of a fixed mass are progressively more clustered towards higher redshift (see also Grazian et al. 2004). Following the approach of Haiman & Hui (2001) and Martini & Weinberg (2001), the estimated quasar lifetime would be a few  $10^7$  yr, reaching  $\sim 10^8$  yr at the highest observed redshifts. More recent studies on larger samples and at different redshifts have confirmed these results (Shen et al. 2007; Myers et al. 2007; Coil et al. 2007; da Ângela et al. 2008; Padmanabhan et al. 2008; Ross et al. 2009). However, the magnitude range covered by these surveys is typically quite narrow, and this may explain the lack of evidence for a significant dependence of clustering on luminosity. When Shen et al. (2008) analyze the clustering of the 10% brightest objects of their sample, they find that these quasars have a higher bias compared to the full sample.

Using hydrodynamical simulations of isolated galaxy mergers (Springel et al. 2005; Di Matteo et al. 2005), Hopkins et al. (2005) studied the luminosity distribution of accreting BHs, whose activity is triggered by the merger event. Hopkins et al. (2005) found that the luminosity distribution of the simulated AGN is equivalent to a highly efficient accretion phase (with very high Eddington ratios), followed by a decaying phase where AGN spend most of their life. During this extended period, they would appear as faint AGN, even though they may, in fact, contain quite massive BHs.

Based on these results, Lidz et al. (2006) explored the dependence of quasar clustering on luminosity, using an analytic approach to connect quasars, black hole masses and halo masses. In a quasar model in which the bright end of the luminosity function is populated by BHs accreting close to their peak luminosity, and the faint end is mainly populated by BHs accreting at low Ed-

dington ratio, there should be no strong dependence of clustering on quasar luminosity, i.e., bright and faint AGN should actually be the same type of objects, but seen in different stages of their evolution. They should therefore be hosted by dark matter haloes of similar masses and hence exhibit similar clustering properties. Assuming a relation between the quasar B-band peak luminosity and the mass of the host haloes, Lidz et al. (2006) tested this prediction, and indeed found that only a narrow range of halo masses should host active quasars, with a median characteristic mass of  $M_{\text{halo}} \sim 1.3 \times 10^{13} M_{\odot}$ . As pointed out by the authors, only future surveys that will be able to observe the faint quasars in their quiescent stage will be able to test this picture, and to rule out the alternative hypothesis of luminosity-dependent quasar clustering.

In the present work we explore the properties of quasar clustering using a semi-analytic model for galaxy formation and BH accretion developed on the outputs of the Millennium Simulation (Springel et al. 2005). Compared to other theoretical work, we do not have to make assumptions about the halo population hosting BHs nor about the relation between the halo mass and the quasar luminosity (or BH mass), since they are a natural outcome of the simulation of the galaxy formation process. However, we have to make assumptions about the physics of BH accretion, and what triggers AGN activity. In this work we are especially interested in testing the assumption that galaxy mergers are the primary physical mechanism responsible for triggering accretion onto massive BHs. To this end we explore the simulation predictions for quasar clustering and the quasar luminosity function obtained with a pure Eddington-limited lifetime model and a model that includes a low-luminosity accretion mode as described by Hopkins et al. (2005) (see also Marulli et al. 2008, hereafter Paper I).

After an introduction to our methodology and a review of some basic properties of our simulated AGN population (Section 2), we show their clustering properties in Section 3, where we also compare our results with the most recent observational optical data available. In Section 4, we show the relation between luminous BHs, quiet BHs and their host haloes. Finally, we summarize and discuss our results in Section 5.

## 2 MODELS FOR BLACK HOLE ACCRETION AND EMISSION

In this Section, after a short overview of our semi-analytic model, we describe the different phases of BH growth and emission adopted in our model. We then review some basic properties of the simulated AGN population; further details are given in Paper I.

### 2.1 From dark matter particles to galaxies

The semi-analytic model used in this work is run on the outputs of the Millennium Simulation (Springel et al. 2005). This is an N-body simulation which follows the cosmological evolution of  $2160^3 \simeq 10^{10}$  dark matter particles, each with mass  $\sim 8.6 \times 10^8 h^{-1} M_{\odot}$ , in a periodic box of  $500 h^{-1} \text{Mpc}$  on a side. The cosmological parameters used in the simulation are the ones of the WMAP1 & 2dFGRS ‘concordance’  $\Lambda$ CDM framework:  $\Omega_m = 0.25$ ,  $\Omega_{\Lambda} = 0.75$ ,  $\sigma_8 = 0.9$ , Hubble parameter  $h = H_0/100 \text{ kms}^{-1} \text{Mpc}^{-1} = 0.73$  and primordial spectral index  $n = 1$  (Spergel et al. 2003).

The merging history trees extracted from this simulation describe the detailed formation history of DM haloes and their subhaloes, identified with a friends-of-friends (FOF) group-finder and

an extended version of the SUBFIND algorithm (Springel et al. 2001), respectively. Using the trees as basic input, our semi-analytic code describes the baryonic processes of galaxy formation and allows the prediction of galaxy properties in a large cosmological volume.

The present work is based on the galaxy formation model described by Croton et al. (2006) and De Lucia & Blaizot (2007), which we extended to follow the details of BH accretion and the lightcurves of AGN. We refer the reader to these papers for a full description of the baryonic physics which describes the evolution of galaxies, their stars and their gas. Below, we describe only the prescriptions that directly relate to our study of the evolution of SMBHs.

## 2.2 Creation and accretion of BHs

In this subsection we discuss our modeling of the physical processes responsible for BH accretion. In the semi-analytic model, a fraction of the mass of a halo is assigned to baryons in the form of hot gas, which as time evolves, will cool and form a galaxy. We also add a ‘seed’ BH of very small mass to each newly formed halo. As galaxies evolve their central BHs are allowed to grow through mergers with other BHs and through gas accretion during the ‘radio mode’ and during the ‘quasar mode’. The quasar mode is the phase during which BHs accrete most of their mass, and during which BHs can shine as bright AGN. We will therefore mainly concentrate most of the discussion on this phase, and we will describe which physical process might be responsible for triggering this activity.

### 2.2.1 BH seeding

The origin of primordial massive BHs is still subject of intense debate: SMBHs seeds could grow out of the remnants of Pop III stars (e.g., Madau & Rees 2001; Heger & Woosley 2002) or could have their origin directly in the collapse of a low-angular momentum gas cloud (e.g., Loeb & Rasio 1994; Koushiappas et al. 2004). In the first case the progenitors of SMBHs would have a mass of the order of  $10^2 - 10^3 M_\odot$ , much less than what could be the outcome of low-angular momentum gas collapse ( $10^5 M_\odot$ ).

Unfortunately, due to exponential growth during accretion, it is very difficult to use the local population of massive holes to recover information about their original mass before the onset of accretion. On the theoretical side, simulations are being carried out to investigate which model for massive BH formation is most plausible (e.g., Bromm & Loeb 2003; Alvarez et al. 2008). Observationally, these models for primordial BHs will hopefully be tested in the near future either directly through gravitational wave detection (Sesana et al. 2005; Koushiappas & Zentner 2006), or indirectly by looking at the effect that primordial BHs might have on reionization (e.g., Ricotti et al. 2005; Ripamonti et al. 2008).

As in Paper I, we assume here that every newly-formed galaxy hosts a central BH of  $10^3 M_\odot$ . This seed BH may then start accreting through the processes described below. Note however that a much larger seed would only influence the BH evolution in our model at very high redshifts, but it would not influence the results in the redshift range of main interest in this paper, simply because the large growth factor soon cancels any information about the seed mass.

### 2.2.2 Radio mode

When a static hot halo has formed around a galaxy, we assume that a fraction of the hot gas continues to accrete onto the central BH, causing low-level ‘radio’ activity in the galaxy center. For clarity, this phase, which is called in jargon *radio mode* because it is associated with the activity of radio galaxies at the centre of galaxy clusters (Best et al. 2005), does not include the powerful emission of FR II radio loud QSOs. Following Croton et al. (2006), the BH mass accretion rate during these phases of *radio mode* activity is postulated to scale as follows:

$$\dot{M}_{\text{BH,R}} = \kappa_{\text{AGN}} \left( \frac{M_{\text{BH}}}{10^8 M_\odot} \right) \left( \frac{f_{\text{hot}}}{0.1} \right) \left( \frac{V_{\text{vir}}}{200 \text{ km s}^{-1}} \right)^3, \quad (1)$$

where  $M_{\text{BH}}$  is the BH mass,  $f_{\text{hot}}$  is the fraction of the total halo mass in the form of hot gas,  $V_{\text{vir}}$  is the virial velocity of the halo and  $\kappa_{\text{AGN}}$  is a free parameter set equal to  $7.5 \times 10^{-6} M_\odot \text{ yr}^{-1}$  in order to reproduce the turnover at the bright end of the galaxy luminosity function. Since  $f_{\text{hot}}$  is approximately constant for  $V_{\text{vir}} \gtrsim 150 \text{ km s}^{-1}$ , the dependence of  $\dot{M}_{\text{BH,R}}$  on this quantity has little effect. Note that the accretion rate given by equation (1) is typically orders-of-magnitude below the Eddington limit. In fact, the total mass growth of BHs in the *radio mode* relative to the *quasar mode* (discussed below) is negligible (Croton et al. 2006).

It is also assumed that *radio mode feedback* injects energy efficiently into the surrounding medium, which can reduce or even stop the cooling flows in halo centers. The mechanical heating generated by this kind of BH mass accretion is parameterized as  $L_{\text{BH}} = \epsilon \dot{M}_{\text{BH}} c^2$ , where  $\epsilon = 0.1$  is the *accretion efficiency* and  $c$  is the speed of light. The heating modifies the infall rate due to cooling according to:

$$\dot{m}'_{\text{cool}} = \dot{m}_{\text{cool}} - \frac{L_{\text{BH}}}{0.5 V_{\text{vir}}^2}. \quad (2)$$

For consistency we never allow  $\dot{m}'_{\text{cool}}$  to fall below zero. In this scenario, the effectiveness of radio AGN in suppressing cooling flows is greatest at late times and for large values of the BH mass, which is required to successfully reproduce the luminosities, colors and clustering of low-redshift bright galaxies.

### 2.2.3 Quasar mode

This is the phase during which BHs accrete cold gas and build up most of their final mass. This phase has recently acquired the jargon name *quasar mode* because it is only through the very efficient accretion of cold gas that a BH can shine as a bright AGN, but we stress that this phase is also meant to include accretion of cold gas at low Eddington ratios.

The tight relation observed locally between BH mass and the host bulge (e.g., Magorrian et al. 1998; Ferrarese & Merritt 2000; Tremaine et al. 2002; Marconi & Hunt 2003) suggests that bulges and BHs might form during the same events and/or they strongly influence each other as they evolve. Simulations have shown that during mergers of gas-rich disk galaxies gas is channeled toward the nuclei of the merging galaxies through gravitational torques (Barnes & Hernquist 1996), and this process can indeed be responsible for the formation of bulges as well as for BH accretion (Springel et al. 2005; Di Matteo et al. 2005).

Based on these results, and following Kauffmann & Haehnelt (2000), in the present work we assume that the quasar phase is triggered by galaxy mergers. In practice, during merger events, we assume that the BHs hosted by the merging galaxies instantaneously

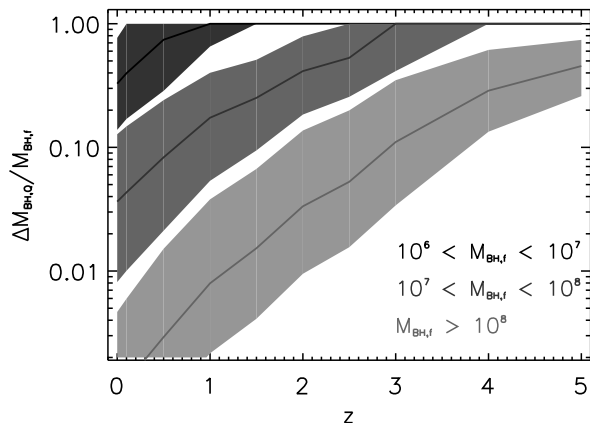


**Figure 1.** Median accreted gas  $\Delta M_{\text{BH,Q}}$  relative to the final BH mass for each accretion event, for three different final mass bins. The filled contours enclose the 25 and 75 percentiles.

coalesce and form a single BH whose mass is the sum of the progenitor BHs, and that this resulting BH starts accreting a fraction of the available cold gas. In Paper I we found that we need to feed BHs more efficiently at high redshifts in order to build massive BHs by  $z = 5$  without invoking super-Eddington accretion or much more massive seed masses. In this work we assume that the amount of cold gas accreted during each merger depends linearly on redshift (Croton 2006):

$$\Delta M_{\text{BH,Q}} = \frac{f'_{\text{BH}} m_{\text{cold}}}{1 + (280 \text{ km s}^{-1} / V_{\text{vir}})^2} (1 + z_{\text{merg}}), \quad (3)$$

where  $m_{\text{cold}}$  is the total mass of cold gas in the final galaxy,  $z_{\text{merg}}$  is the redshift of the merger and

$$f'_{\text{merg}} = f_{\text{merg}} (m_{\text{sat}} / m_{\text{central}}), \quad (4)$$

where  $f_{\text{merg}} \approx 0.02$  is a normalization parameter chosen to match the observed local  $M_{\text{BH}} - M_{\text{Bulge}}$  relation and  $m_{\text{sat}} / m_{\text{central}}$  is the mass ratio of the merging galaxies.

In Figure 1 we show, as a function of redshift, the median accreted mass  $\Delta M_{\text{BH,Q}}$ , relative to the value of the BH mass at the end of a single accretion event, for three final mass bins. Small-mass BHs accrete efficiently at all epochs (higher curve), whereas BHs that, at the end of the accretion event, end-up in massive objects (lower curve) accrete most of their mass at early times: at low-redshifts, the amount of ‘new’ gas accreted is relatively small compared to the mass already acquired. This behavior is in agreement with the apparent ‘anti-hierarchical’ growth of BHs: observations in the soft and hard X-rays have shown that the number density of bright AGN declines with decreasing redshift, while the density of fainter active nuclei shows the opposite trend (Cowie et al. 2003; Steffen et al. 2003; Ueda et al. 2003; Hasinger et al. 2005). Heckman et al. (2004) used the emission lines of type 2 AGN observed with SDSS to investigate whether the decrease of the space density of bright objects is simply due to a decrease in the accretion rate or a decrease in the typical mass of actively growing BHs. These authors found that the typical mass of BHs that are today actively accreting is  $\lesssim 10^7 M_{\odot}$ , and that larger BHs are experiencing little accretion.

In Paper I we showed that, at  $z = 0$ , this model for BH accretion is able to reproduce not only the observed  $M_{\text{BH}} - M_{\text{Bulge}}$  relation (Haring & Rix 2004), but also other scaling relations, such as the ones between the BH mass and the galaxy central velocity dispersion or color (Marconi & Hunt 2003; Ferrarese & Ford

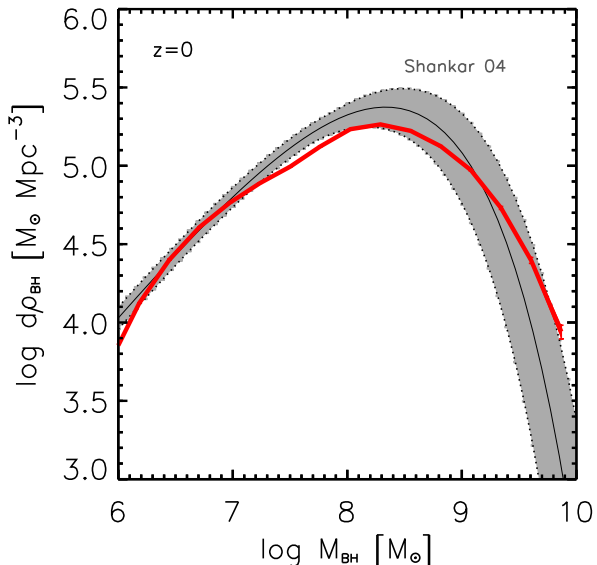


**Figure 2.** Differential BH mass density at  $z = 0$  (red thick line) compared to the observational estimate of Shankar et al. (2004) (solid black line, with errors enclosed in the grey shaded area).

2005). The  $z = 0$  differential mass density of our simulated BHs is shown in Figure 2 compared with the observational estimate of Shankar et al. (2004). The corresponding local mass density (for our cosmology with  $h = 0.73$ ) is  $\rho_{\text{BH}} = 3.35 \times 10^5 M_{\odot} \text{ Mpc}^{-3}$ , which is in good agreement with Graham & Driver (2007) (we refer to these authors for a summary of the values quoted in the literature).

To study the redshift evolution of the BH population, it is important to not only to consider the evolution of the BH mass, but also to relate this to the radiation output of the accretion. If we are interested in the instantaneous brightness of a quasar, we not only need to calculate how much mass it accretes, but also how long this takes. In other words, we need to model the lightcurve of individual phases of quasar activity. In Paper I we introduced and tested different models for the AGN lightcurve, and we compared our results with the AGN bolometric luminosity function of Hopkins et al. (2007). We here briefly describe the lightcurve models adopted for the present study.

At any given time, the bolometric luminosity emitted by an accreting BH is given by

$$\begin{aligned} L_{\text{bol}}(t) &= \epsilon \dot{M}_{\text{accr}}(t) c^2 = \frac{\epsilon}{1 - \epsilon} \dot{M}_{\text{BH}}(t) c^2 \\ &= f_{\text{Edd}}(t) L_{\text{Edd}}(t) = f_{\text{Edd}} \frac{M_{\text{BH}}(t)}{t_{\text{Edd}}} c^2, \end{aligned} \quad (5)$$

where  $\epsilon$  is the radiative efficiency,  $L_{\text{Edd}}$  is the Eddington luminosity,  $f_{\text{Edd}}$  is the fraction of Eddington luminosity emitted, and  $t_{\text{Edd}} = \sigma_{\text{T}} c / (4\pi m_p G) \sim 0.45 \text{ Gyr}$  (note that we are here considering only the luminosity emitted during the *quasar mode* phase, thus ignoring the contribution from  $\dot{M}_{\text{BH,R}}$ ). If, at any given time, the radiative efficiency and the Eddington ratio are known, the accretion rate is given by:

$$d \ln M_{\text{BH}}(t) = \frac{dt}{t_{\text{ef}}(t)}, \quad (6)$$

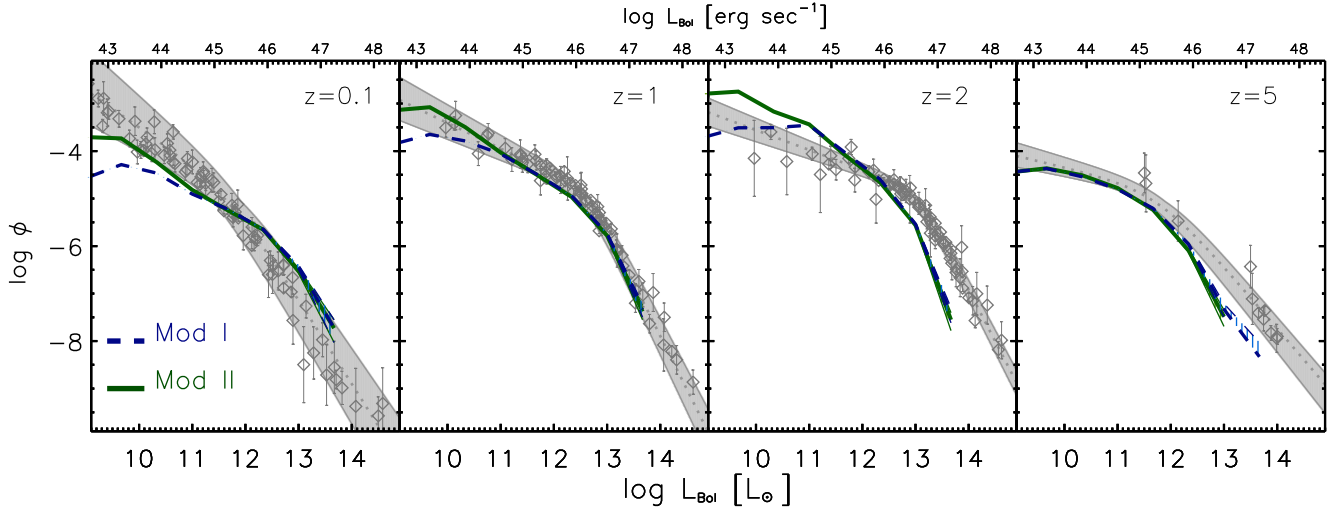


**Figure 3.** Bolometric luminosity function assuming Eddington-limited accretion (Mod I, blue-dashed curve), or Eddington-limited accretion followed by a quiescent phase of low luminosity (Mod II, green-solid curve), with errors calculated using Poisson statistics. The luminosity functions are compared with the compilation of Hopkins et al. (2007) (grey points with best fit given by the grey band).

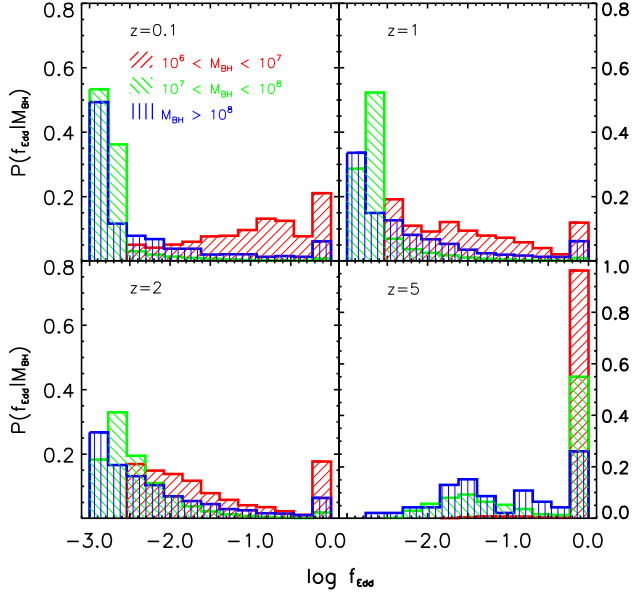


**Figure 4.** Probability distribution of  $f_{\text{Edd}}$  as a function of BH mass and redshift. The limits in the BH mass bins are shown in the first panel in units of  $M_{\odot}$ . At high redshift, most of the BHs accrete at the Eddington limit. Today, only the smallest BHs are experiencing efficient accretion.

where  $t_{\text{ef}}(t) = \frac{\epsilon}{1-\epsilon} \frac{f_{\text{Edd}}}{f_{\text{Edd}}(t)}$  is the e-folding time ( $t_{\text{ef}} \equiv t_{\text{Salpeter}}$  if  $f_{\text{Edd}} = 1$ ).

For simplicity, we assumed a constant radiative efficiency  $\epsilon = 0.1$  (average value for a thin accretion disk, Shakura & Sunyaev 1973), and we explored different models for the time-evolution of  $f_{\text{Edd}}$ . In this work we choose not to explore all the four models discussed in Paper I. Instead, we will focus on two of them, which we regard as representative cases. The first one illustrates the simple

case of an AGN that shines at the Eddington luminosity. It represents a very simple model commonly used in the literature, that we regard as a reference case, despite the fact that, as shown in Paper I, fails to reproduce the AGN luminosity function at low and high redshifts. The second model is very close to the model called 'best' in Paper I and illustrates the impact of adopting a non trivial AGN light-curve, motivated by numerical experiments. As discussed in Paper I this second model provides a better fit to the AGN luminosity function. In what follows, we present a more detailed description of the two models:

- *Model I:*  $f_{\text{Edd}}(t) = \text{const} = 1$ . This is the simplest case, in which we assume that, when active, BHs accrete and radiate at the Eddington limit.
- *Model II:* Here we assume that BHs undergo an Eddington-limited phase that leads to a peak luminosity  $L_{\text{peak}}$ , which is then followed by a long quiescent phase at progressively lower Eddington ratios. Following the work of Hopkins et al. (2005), we assume that in this long quiescent phase the average time that an AGN spends in a logarithmic luminosity interval can be approximated by:

$$\frac{dt}{d \ln L_{\text{bol}}} = |\alpha| t_9 \left( \frac{L_{\text{bol}}(t)}{10^9 L_{\odot}} \right)^{\alpha}, \quad (7)$$

where  $t_9 \equiv t_Q(L' > 10^9 L_{\odot})$  and  $t_Q(L' > L)$  is the total AGN lifetime above a given luminosity  $L$ . Hopkins et al. (2005) found from merger simulations that  $t_9 \sim 10^9$  yr over the range  $10^9 L_{\odot} < L_{\text{bol}} < L_{\text{peak}}$ ; here, we assume always  $t_9 = 10^9$  yr. In the range  $10^{10} L_{\odot} \lesssim L_{\text{peak}} \lesssim 10^{14} L_{\odot}$ , Hopkins et al. (2005) also found that  $\alpha$  is a function of only the AGN luminosity at the peak of its activity,  $L_{\text{peak}}$ , given by  $\alpha = -0.95 + 0.32 \log(L_{\text{peak}}/10^{12} L_{\odot})$ , with  $\alpha = -0.2$  as an upper limit.

In this scenario, the peak luminosity  $L_{\text{peak}}$  reached at the end of the first accretion phase is  $L_{\text{Edd}}(M_{\text{BH,peak}})$ , where

$$M_{\text{BH,peak}} = M_{\text{BH}}(t_{\text{in}}) + \mathcal{F} \cdot \Delta M_{\text{BH,Q}} \cdot (1 - \epsilon). \quad (8)$$

Here  $M_{\text{BH}}(t_{\text{in}})$  is the BH mass at the beginning of the accretion,

$\Delta M_{\text{BH,Q}}$  is the fraction of cold gas mass accreted, and  $\mathcal{F}$  sets the fraction of gas that is accreted during the Eddington-limited phase. After this first phase, the BH keeps accreting the remaining cold gas at a progressively slower rate, as described by equation (7). In Paper I we set  $\mathcal{F} = 0.7$ , a value that balances the needs of efficiently building-up massive BHs and of explaining low- $f_{\text{Edd}}$  BHs in the local universe. Most of the available gas is therefore accreted during the Eddington-limited phase, and the lightcurve model introduced by Hopkins et al. (2005) is used to describe only the quiescent phase.

A direct comparison of the luminosity functions obtained using Mod I and Mod II is shown in Figure 3. Mod I and Mod II give a similar population of high-luminosity AGN: bright AGN are always produced by BHs accreting close to the Eddington limit. At high redshifts, the faint-end of the luminosity function produced by the two models is very similar as well, suggesting that at very high redshifts BHs of all masses typically accrete at  $f_{\text{Edd}} = 1$ . It is in the faint-end of the luminosity function at low redshifts where the two models predict a different behavior for the AGN luminosity: only Mod II (with  $\mathcal{F} = 0.7$ ) is able to fit the low-redshift faint-end of the luminosity function, implying that a model in which BHs experience long, quiescent accretion phases can indeed explain the number density of low-luminosity AGN at low redshift. This is because in Mod II the average lifetime of AGN is much higher (a larger fraction of time is spent at low luminosities); it is therefore more probable to observe, at a given redshift, an AGN shining at low luminosities. For a more detailed discussion on this, we refer again the reader to Paper I.

We have already mentioned that observations indicate that the more massive BHs have accreted most of their mass at early times, whereas in the local universe BHs with a mass  $\lesssim 10^7 M_{\odot}$  are accreting efficiently (Heckman et al. 2004). These results have been confirmed more recently by Netzer & Trakhtenbrot (2007), who found that at all redshifts  $f_{\text{Edd}}$  is smaller for larger mass BHs. Similar compilations that use emission lines to estimate Eddington ratios have shown that the  $f_{\text{Edd}}$  of quasars seems to be log-normally distributed, with a peak around  $f_{\text{Edd}} \approx 10^{-1} - 10^{-0.6}$  (Kollmeier et al. 2006; Shen et al. 2008). In Figure 4 we show, for Mod II, the redshift evolution of the probability distribution  $P(f_{\text{Edd}}|M_{\text{BH}})$  of the Eddington ratios, given the BH mass. At high redshifts all BHs accrete close to the Eddington limit. At lower redshifts instead only the smaller BHs are accreting at high Eddington ratios, while the more massive ones accrete at much lower rates. Note that this figure includes all active BHs from our simulation, and therefore a direct comparison with observed data is not possible. We postpone a more detailed analysis of this point to a future work, but we stress that a model with a quiescent phase could account for the low-redshift behavior of the more massive BHs (see also the recent work of Hopkins & Hernquist 2008).

### 3 CLUSTERING PROPERTIES

In this section we discuss the clustering properties of our simulated AGN sample. We first compare the predicted two-point correlation with the autocorrelation of the DM particles. We then compare the AGN clustering properties with the clustering of the dark matter haloes of the Millennium simulation, and in particular examine the differences between Mod I and Mod II. We then explore the luminosity dependence of the clustering of the global AGN population and of an optically-visible sub-sample. Finally, we directly com-

pare the clustering of our simulated  $L_*$  quasars with recent observational results.

#### 3.1 Brief description of the correlation parameters used

We use the standard definition of the *two-point spatial correlation function* as the excess probability for finding a pair of objects at a distance  $r$ , each in the volume element  $dV_1$  and  $dV_2$  (e.g., Peacock 1999):

$$dP = n^2 [1 + \xi(r)] dV_1 dV_2, \quad (9)$$

where  $n$  is the average number density of the set of objects under consideration.

The *clustering length*  $r_0$  is defined as the scale at which the two-point correlation function is unity:  $\xi(r_0) \equiv 1$  (i.e., the scale at which the probability of a pair is twice the random). At scales between  $\sim 1 h^{-1}\text{Mpc}$  up to few tens of Mpc the observed quasar correlation function can be approximated by a power-law, usually expressed as:

$$\xi(r) = \left(\frac{r}{r_0}\right)^{-\gamma}. \quad (10)$$

To calculate  $r_0$ , unless otherwise stated, we will fit the two-point correlation with such a power-law in the range  $1 < r < 20 h^{-1}\text{Mpc}$  (see the next subsection for details on this).

Finally, the *bias* between two classes of objects (e.g., AGN and dark matter) is defined as the square-root of the ratio of the corresponding two-point correlation functions:

$$b_{\text{AGN,DM}} \equiv \sqrt{\frac{\xi_{\text{AGN}}(r)}{\xi_{\text{DM}}(r)}}. \quad (11)$$

In principle, an accurate determination of the ‘cosmic variance’ errors of these quantities as measured from the simulation could be calculated from the variance over many different realizations of the universe. As we have only one simulation as large as the Millennium run at our disposal, this is not practical. A reasonable alternative is to estimate the errors by subdividing the whole Millennium volume into sub-cubes, and then by calculating the variance among the measurements for each of these sub-volumes, an approach we will follow here.

In order to directly estimate the impact of the cosmic variance in the predicted AGN clustering, it is necessary to model the AGN properties in mock samples designed to match the real ones. We have followed this approach in a parallel work (Marulli et al. (2009), submitted to MNRAS), where we have used the same semi-analytic model presented here to construct mock AGN catalogues mimicking the Chandra deep fields.

#### 3.2 AGN and dark matter clustering

We here show the results for the shape of the two-point correlation of the AGN sample, comparing it to the one of the Millennium dark matter particles. For simplicity, we present only the results obtained with Mod II, since the conclusions of this subsection are independent of the assumed model for the lightcurve.

In the top panels of Figure 5, we plot the two-point correlation of the DM particles (dotted line) and the two-point correlation of faint ( $L_{\text{Bol}} < 10^{10} L_{\odot}$ ) and bright ( $L_{\text{Bol}} > 10^{11} L_{\odot}$ ) AGN (dashed lines), at three different redshifts. As can be seen at a glance, the main difference between  $\xi_{\text{DM}}(r)$  and  $\xi_{\text{AGN}}(r)$  lies in the normalization, they are substantially biased relative to each

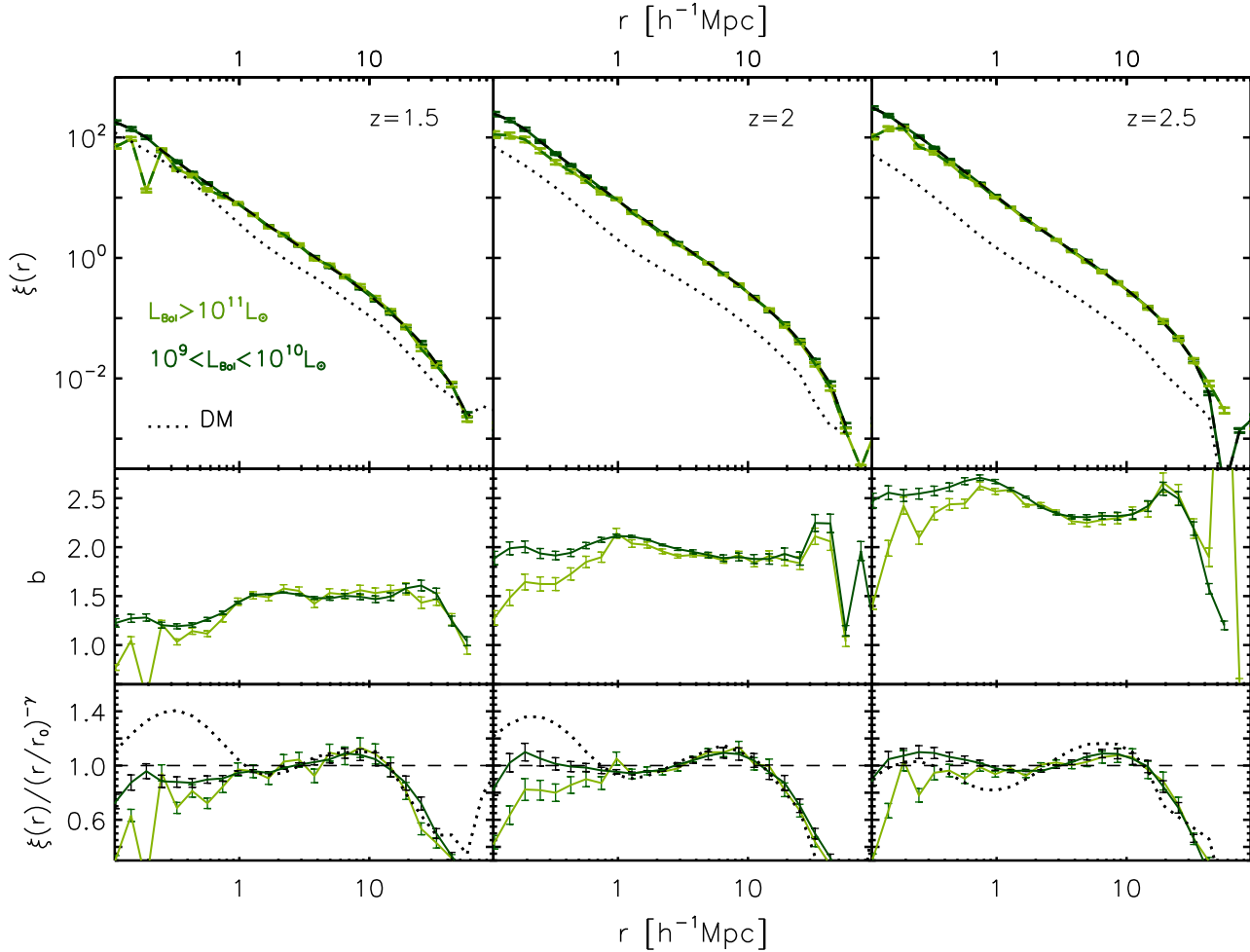


**Figure 5.** *Upper panels:* two-point correlation function of the Millennium dark matter particles (dotted line) compared with the correlation of the AGN population, divided into a faint and a luminous sub-sample, depending on their bolometric luminosity (as indicated in the first panel). *Central panels:* bias between the two AGN samples and the dark matter as a function of scale. *Lower panels:* two-point correlation from the upper panels divided by a power-law fit. If  $\xi(r)$  was a perfect power-law, the ratio should be constant with scale and equal to unity (dashed horizontal line). We refer to the text for a description of the errors.

other. This bias ( $[\xi_{\text{AGN}}(r)/\xi_{\text{DM}}(r)]^{1/2}$ ) is plotted in the next set of panels of Fig. 5. The bias is approximately scale-independent (at least in the range  $1 < r < 20 h^{-1}\text{Mpc}$ ), and its average value increases with redshift. The error  $\sigma_{\log \xi_{\text{AGN}}}(r)$  of the two-point correlation is here the variance (in log-space) of the two-point correlation functions calculated in eight sub-volumes. The errors on the bias have been calculated assuming negligible error for DM autocorrelation. By error propagation, the error on the bias is then  $\sigma_b(r) = b(r) \sigma_{\log \xi_{\text{AGN}}}(r) (\ln 10)/2$ .

Finally, in the lower panels of Fig. 5 we show how the two-point correlations deviate from a power-law, that is, we divide the calculated  $\xi(r)$  by the fit calculated using eq. (10). As is well known (e.g. Springel et al. 2005), the DM correlation function deviates from a pure power-law at low and intermediate scales. The AGN correlation function shows a similar shape at intermediate scales ( $r \sim \text{few } h^{-1}\text{Mpc}$ ), but not at small scales, where the AGN two-point correlation function is a significantly ‘better’ power-law than that of the DM. This is highly reminiscent of the findings for the clustering of galaxies (Springel et al. 2005).

As we will again see in the next subsection, the lack of a strong

correlation signal at small scales is due to the fact that our BHs accrete gas and can shine as bright AGN only after merger events, which, in our model, happen mainly in the central galaxies of dark matter haloes (whose mean separation is  $\approx 1 h^{-1}\text{Mpc}$ ). Also note that each of our mergers lights up only one BH, the merged BH of the two progenitor galaxies, i.e. our model does not account for the possibility that the two BHs exhibit activity as a close quasar pair already prior to coalescence. Also, as a BH is still accreting cold gas, it can happen that its host halo merges with another halo which could have at its center another accreting BH. This is also why the correlation power at scales  $\lesssim 1 h^{-1}\text{Mpc}$  is non-zero, but negligible. In a forthcoming paper we will compare a pure merger-triggered AGN scenario, with a model in which the possible galaxy disk instability also could contribute in feeding BHs. In this last case we expect a larger AGN halo occupation distribution (number of AGN in a single halo), and a different behavior in the small-scale clustering regime.



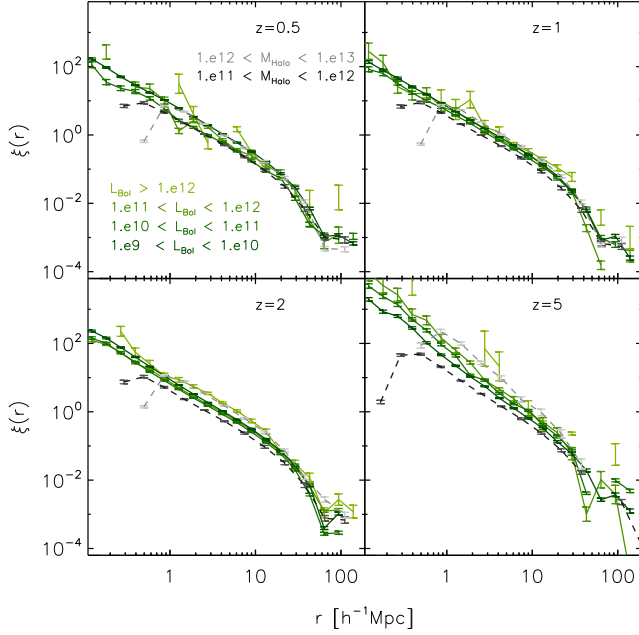


**Figure 6.** Two-point correlation function for the AGN sample compared to the two-point correlation of the Millennium FOF haloes, at various redshifts. The AGN are divided into 4 luminosity bins (depending on the bolometric luminosity), whereas the haloes are divided into two bins, depending on the value of their virial mass in units of  $h^{-1}M_{\odot}$ . The AGN in this figure have been obtained using Mod II for the lightcurve. In Figure 8, the main difference in the correlation between the two models is highlighted.

### 3.3 AGN and halo clustering

In this subsection we compare the AGN clustering with the clustering of the Millennium haloes. In our model, BHs are allowed to accrete cold gas only during merger events, which are experienced mainly by the galaxies sitting at the centers of FOF haloes. As discussed above, only a small fraction of AGN can be hosted by satellite haloes. Due to this uncertainty in the quasar pair regime, we focus in the present work on the clustering on intermediate and large scales, and we refrain from drawing strong conclusions from the results at scales much smaller than the average halo separation.

In Figure 6, we show at different redshifts the two-point correlation function of the AGN population, divided in four luminosity bins depending on their intrinsic bolometric luminosity. This is compared with the two-point correlation of the FOF haloes, divided into two bins according to their virial mass. The AGN shown in this figure have been obtained using Mod II for the lightcurve. The corresponding correlation lengths are shown in the lower panel of Figure 7. In the upper panel of the same figure the correlation lengths of the AGN obtained using Mod I are plotted, also divided in four luminosity bins. In the analysis of the results, we allow the exponent  $\gamma$  of the power-law ansatz for the correlation function to vary in each fit. The values of  $r_0$  and  $\gamma$  for the two models thus obtained are given in Tables 1 and 2. We also fitted the brightest bin with a quadratic function ( $r_0(z) = a + b(1+z) + c(1+z)^2$ ) to compactly summarize the results, and the values of the coefficients are given at the end of each table.

Comparing the values of the correlation lengths obtained with the two models, we do not find significant differences, except for the faintest AGN ( $L_{\text{Bol}} < 10^{10}L_{\odot}$ ). An enlarged view of the behavior of the correlation strength of these faint objects obtained with

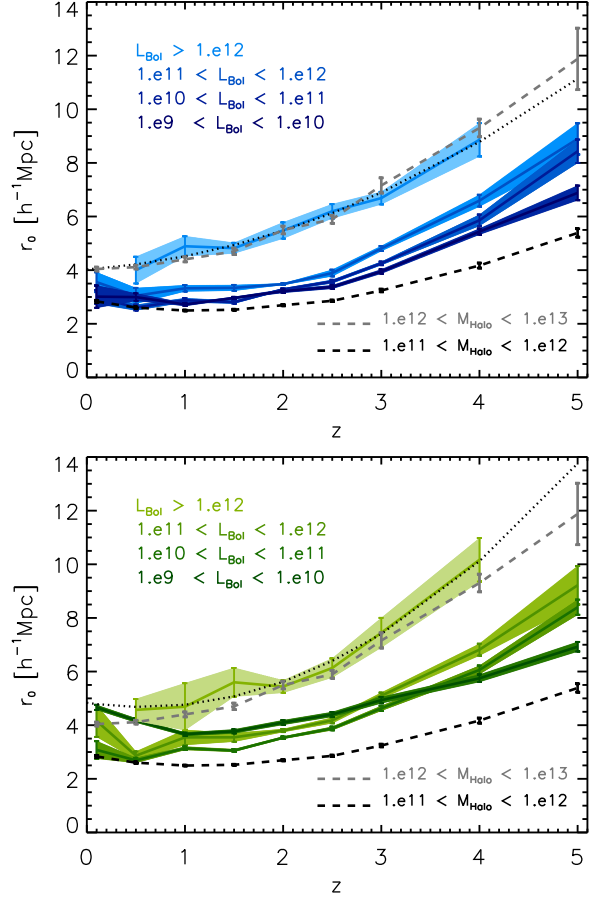


**Figure 7.** Correlation length as a function of redshift of the AGN sample divided in four bolometric luminosity bins, compared with the correlation length of the length of two mass bins of the Millennium FOF haloes. The AGN have been obtained using Mod I (upper panel) or Mod II (lower panel) as lightcurve models, respectively. Fits to the brightest bins are shown with the dotted curve.

Mod I (solid blue curve) and with Mod II (dotted green curve) is shown in Figure 8. While at high redshifts there is hardly any difference between the two models, at low redshift the faint objects obtained with Mod II are much more strongly clustered. This is because most of the population is composed of large BHs that are accreting at low  $f_{\text{Edd}}$  (as shown in Figure 4) and that are hosted by large haloes. In the lower panel of Figure 8, we see that the correlation length of the faint objects obtained with Mod II is comparable to the ones of haloes with  $M_{\text{Vir}} \approx 10^{12} - 10^{13}M_{\odot}$ , while faint objects obtained with a pure Eddington-limited accretion model are sitting in haloes of much lower mass. Observational clustering measurements have been used in recent years to estimate the typical halo masses that host quasars (e.g., Porciani et al. 2004; Grazian et al. 2004; Croom et al. 2005). This is usually done by comparing the bias of observed quasars with the halo bias obtained from analytical estimates (Mo & White 1996; Sheth & Tormen 1999, e.g.). In the present work, the host halo mass is an output of the simulation, and therefore we can directly examine the relation between black hole mass, quasar luminosity and halo mass. In section 4, we exploit this for a direct study of the dark environment of luminous BHs.

Based on Figure 7, it seems that the redshift-evolution of the



Mod I									
$L_1$			$L_2$		$L_3$		$L_4$		
$z$	$r_0$	$\gamma$	$r_0$	$\gamma$	$r_0$	$\gamma$	$r_0$	$\gamma$	
0.1	-	-	$3.55 \pm 0.37$	1.4	$3.0 \pm 0.26$	1.79	$3.01 \pm 0.42$	1.5	
0.5	$4.0 \pm 0.5$	1.69	$3.04 \pm 0.29$	1.49	$2.6 \pm 0.11$	1.53	$3.0 \pm 0.14$	1.49	
1.0	$4.89 \pm 0.37$	1.62	$3.32 \pm 0.12$	1.63	$2.88 \pm 0.08$	1.5	$2.72 \pm 0.06$	1.52	
1.5	$4.82 \pm 0.2$	1.79	$3.34 \pm 0.11$	1.57	$2.81 \pm 0.06$	1.56	$2.96 \pm 0.04$	1.57	
2.0	$5.48 \pm 0.3$	1.71	$3.48 \pm 0.03$	1.55	$3.28 \pm 0.04$	1.55	$3.22 \pm 0.06$	1.5	
2.5	$6.2 \pm 0.27$	1.54	$3.89 \pm 0.12$	1.58	$3.57 \pm 0.07$	1.54	$3.37 \pm 0.07$	1.55	
3.0	$6.69 \pm 0.23$	1.79	$4.81 \pm 0.09$	1.6	$4.25 \pm 0.06$	1.59	$3.95 \pm 0.08$	1.57	
4.0	$8.86 \pm 0.62$	1.77	$6.59 \pm 0.22$	1.76	$5.86 \pm 0.21$	1.7	$5.44 \pm 0.11$	1.66	
5.0	-	-	$8.89 \pm 0.58$	2.04	$8.43 \pm 0.44$	1.89	$6.88 \pm 0.27$	1.81	

fit for  $L_1: r_0 = a + b(1+z) + c(1+z)^2$ , with  $a, b, c = [4.01, -0.21, 0.23]$

**Table 1.** Values of the correlation lengths shown in the upper panel of Figure 7. We also added the values of the corresponding power-law slope  $\gamma$ .  $L_1$  corresponds to the brightest bin,  $L_4$  to the faintest. We also give the values of the parameters of the quadratic fit done on  $r_0$  for the brightest bin.

Mod II									
$L_1$			$L_2$		$L_3$		$L_4$		
$z$	$r_0$	$\gamma$	$r_0$	$\gamma$	$r_0$	$\gamma$	$r_0$	$\gamma$	
0.1	-	-	$4.15 \pm 0.6$	1.69	$3.08 \pm 0.33$	1.72	$4.66 \pm 0.09$	1.61	
0.5	$4.57 \pm 0.96$	1.96	$2.86 \pm 0.15$	1.27	$2.69 \pm 0.1$	1.45	$4.18 \pm 0.08$	1.58	
1.0	$4.69 \pm 0.88$	1.62	$3.55 \pm 0.28$	1.58	$3.14 \pm 0.06$	1.51	$3.67 \pm 0.07$	1.56	
1.5	$5.6 \pm 0.53$	1.89	$3.55 \pm 0.16$	1.52	$3.05 \pm 0.05$	1.53	$3.77 \pm 0.07$	1.56	
2.0	$5.44 \pm 0.23$	1.68	$3.8 \pm 0.06$	1.54	$3.53 \pm 0.04$	1.56	$4.1 \pm 0.09$	1.58	
2.5	$6.13 \pm 0.36$	1.52	$4.18 \pm 0.11$	1.57	$3.88 \pm 0.07$	1.56	$4.4 \pm 0.09$	1.59	
3.0	$7.45 \pm 0.55$	1.72	$5.1 \pm 0.11$	1.65	$4.63 \pm 0.09$	1.6	$4.94 \pm 0.12$	1.64	
4.0	$10.17 \pm 0.81$	1.82	$6.82 \pm 0.22$	1.77	$6.06 \pm 0.16$	1.77	$5.75 \pm 0.14$	1.72	
5.0	-	-	$9.22 \pm 0.72$	2.01	$8.4 \pm 0.28$	1.87	$6.93 \pm 0.18$	1.84	

fit for  $L_1: r_0 = a + b(1+z) + c(1+z)^2$ , with  $a, b, c = [5.84, -1.47, 0.46]$

**Table 2.** Same as the previous table, this time for the AGN obtained with Mod II (lower panel of Figure 7).

clustering of quasars is consistent with the redshift-evolution of the clustering of dark matter haloes (quasars of a given luminosity reside at all times in haloes of a fixed mass). Again, the only substantial difference to this trend is for the faint objects obtained with Mod II: since their clustering is more constant with redshift, it implies that their typical host halo mass changes with redshift.

### 3.4 Luminosity dependence of AGN clustering and comparison with observational data

In this subsection we first examine the dependence of AGN clustering on luminosity, looking at the global population, and then considering a subsample that would be observable in the optical band.

Observationally, quasar clustering seems not to depend significantly on luminosity (Porciani et al. 2004; Croom et al. 2005; da Ângela et al. 2008, e.g.). Only Shen et al. (2008) found indications of a luminosity-dependence of the clustering when they compared the two-point correlation of their 10% brightest objects with the rest of the sample. Figure 7 provides information on how the correlation length evolves with luminosity in our models. Except for the faintest bin (see Figure 8), there is not a substantial difference between the two models, as pointed out before. In both models we see some moderate evolution with luminosity, and in particular,

in both cases the brightest quasar bin is substantially more strongly clustered than the lower luminosities.

Note that in this analysis a very large range in luminosities is covered ( $\approx 5$  dex in luminosity, corresponding to  $\approx 12.5$  absolute magnitudes). Observationally, the accessible luminosity range is always much smaller than that. To give predictions that can be compared with future observations, we now extract from the global AGN population sub-samples of optically visible bright AGN. First of all, to account for obscuration, we calculate the fraction of objects that would be visible in the optical using the ‘observable fraction’ from Hopkins et al. (2007). This gives, as a function of luminosity, the probability for an object to be seen in a given band:

$$f(L) = f_{46} \left( \frac{L}{10^{46} \text{ergs}^{-1}} \right)^\beta, \quad (12)$$

where  $f_{46} = 0.260$  and  $\beta = 0.082$ ) for the B-band.

To convert from bolometric luminosity to B-band luminosity, we used the bolometric corrections again from Hopkins et al. (2007):

$$\frac{L_{\text{bol}}}{L_{\text{band}}} = c_1 \left( \frac{L_{\text{bol}}}{10^{10} L_\odot} \right)^{k_1} + c_2 \left( \frac{L_{\text{bol}}}{10^{10} L_\odot} \right)^{k_2}, \quad (13)$$

where  $(c_1, k_1, c_2, k_2)$  are respectively  $(6.25, -0.37, 9.0, -0.012)$  for the B-band.

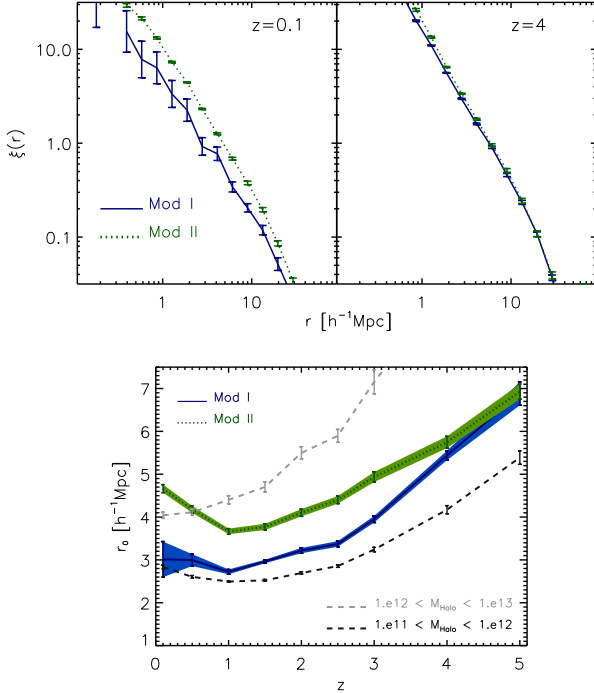


**Figure 8.** We compare here the correlation function of faint AGN ( $L_{\text{Bol}} < 10^{40} L_{\odot}$ ) obtained using Mod I (solid blue line) and Mod II (dotted green line). We show the result at very high redshift, where there is no difference in the two models, and at low redshift, where the difference becomes significant. In the lower panel the corresponding correlation function is shown as a function of redshift, and the correlation of FOF haloes is shown for reference.

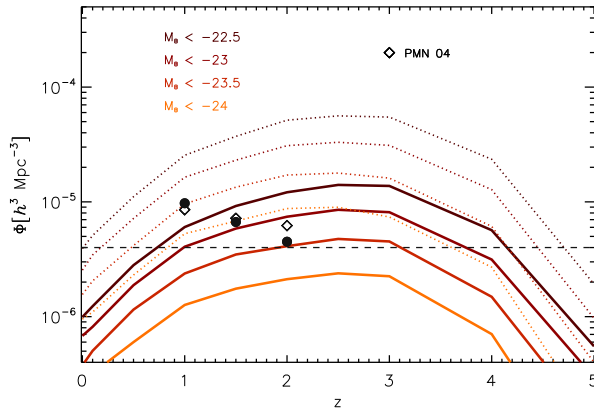


**Figure 9.** Space density as a function of redshift for four subsamples selected with B-band magnitude cuts as indicated on the plot. The solid lines are give the space density when the possible obscuration is taken into account. If we allow all our objects to be optically visible, we obtain the space densities described by the dotted curves. The dashed line marks the point below which we have less than 500 objects remaining in in the Millennium simulation volume. The open diamonds are the observed values from Porciani et al. (2004), obtained in different magnitude ranges depending on the redshift (see text for details). The number densities obtained with our model using the same magnitude ranges and accounting for obscuration are indicated with the filled circles.

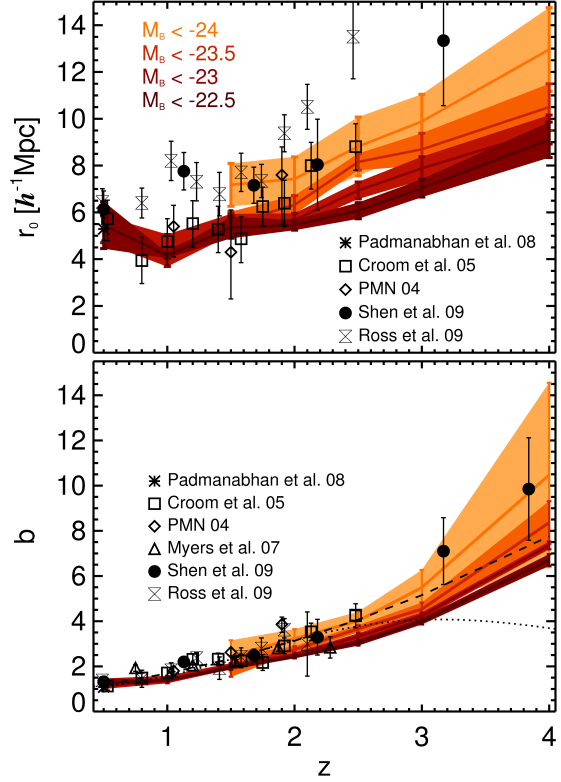


**Figure 10.** Correlation length (top panel) and bias (lower panel) for the AGN selected using the cuts of Figure 9 (neglecting the effects of obscuration). Due to lack of enough objects, the clustering properties of the two brightest bins are calculated only down to  $z = 1.5$ . Our predictions are plotted together with observational data (for the Shen et al. (2008), we included their lower estimates). For the bias, the dotted line is the prediction of Hopkins et al. (2007) and the short-dashed line is the best fit from Croom et al. (2005).

In Figure 9 we show as a function of redshift the number density of our simulated AGN for different luminosity cuts (solid lines). In order to directly compare our number densities with the values inferred from observational data used for clustering measurements, we calculated in the same figure the number density of objects in the magnitude ranges given by Porciani et al. (2004) at three different redshifts: the values of  $M_{\text{min}}$  and  $M_{\text{max}}$  are  $[-25.32, -21.72]$  at  $z \sim 1.0$ ,  $[-25.97, -22.80]$  at  $z \sim 1.5$ , and finally  $[-26.44, -23.37]$  at  $z \sim 2.0$  (see their Table 1). Note that their value are in  $b_J$ , and to convert from  $B$  to the  $b_J$ -band we used the relation given by these authors in their Appendix 1, where  $M_B = M_{b_J} + 0.07$ . In the Figure, our points are the black dots, while the numbers quoted by Porciani et al. (2004) are shown with diamonds (the errors quoted by these authors are comparable to the size of the symbol, and therefore are omitted). The agreement is quite good, even though we slightly underestimate the number of bright quasars at  $z = 2$ , as expected (see the bright-end of the luminosity function at this redshift in Figure 3). In Figure 9 we also show the number density of our simulated AGN for the same luminosity cuts, but without accounting for obscuration (dotted lines). As described above, we account for obscuration by calculating for each object its probability of being optically visible and then by randomly extracting objects that satisfy the imposed condition. Since this probability is a weak function of luminosity, and since

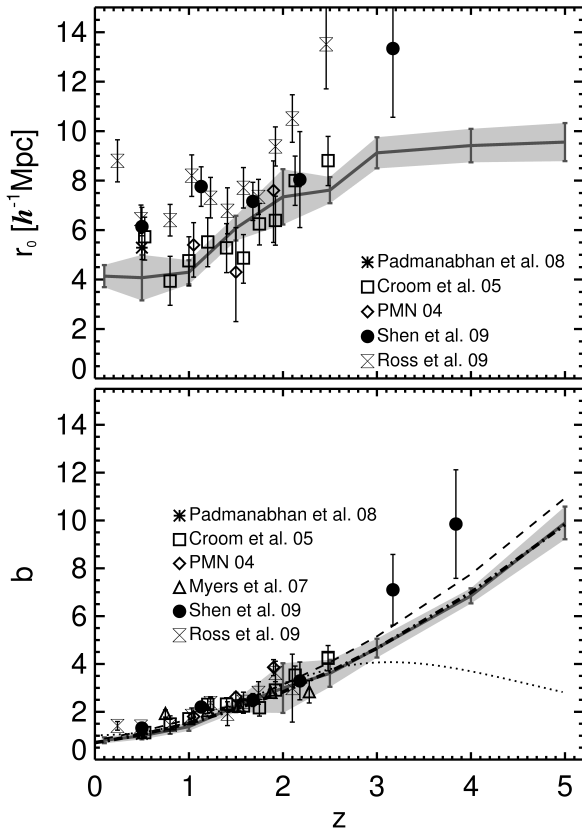


**Figure 11.** Correlation length (top panel) and bias (lower panel) for  $L_*$  quasars. The gray line is our prediction (with errors enclosed in the grey area). The observational data are the same of Figure 10. A fit to our predicted bias as a function of redshift is given in equation (14).

clustering analysis is independent of random sampling, for our study we ignore the effect of obscuration. This allows us to push the analysis to brighter magnitude cuts, since for a statistically-accurate clustering analysis we need at least few hundred objects (the dashed horizontal line shows the point at which, in the full simulation volume, we cannot expect more than 500 objects).

The correlation lengths of the AGN selected with these luminosity cuts are shown in Figure 10. We see that at low and intermediate redshifts the correlation length and the bias depend weakly on luminosity when a narrow range of luminosities is examined. Since bright quasars are always powered by BHs accreting close to the Eddington limit, it seems difficult to use quasar clustering observations to disentangle between different light-curve models, unless much larger luminosity ranges are probed. The present observations indicate however that, over the range of luminosities observed, quasars reside in haloes of similar masses. Based on our results, we conclude that the lack of a significant dependence of clustering on luminosity is not primarily a result of invoking lightcurve models with a wide distribution of Eddington ratios, but rather arises because in a merger-driven scenario there is a small scatter in the typical halo mass hosting quasars close to their peak luminosity.

In Figure 10 we added observational data from several works, to qualitatively compare our results with observations. We stress though that the error bars in these figures are calculated to describe the effect of cosmic variance as described in Section 3.1; since we are here ignoring the effect of obscuration, thus improv-

ing our statistic, a direct comparison with the error bars given by observational works is not possible.

Most of the observed quasars have a typical magnitude around  $M_{b_j}^*$  (Croom et al. 2005), with faint limits that strongly depend on redshift (at very low redshifts surveys can reach fainter magnitudes, whereas at very high redshifts the limiting magnitudes can be higher than  $M_*$ ). At  $z \lesssim 1$  the faintest observed magnitudes are  $M_B \approx -22$ , going up to  $\approx -24$  at  $z \sim 2-3$ . Since each observational study uses different magnitude cuts, we can not do a detailed comparison with all the observations available, but overall our results for the values of the correlation length and the bias and their evolution with redshift are in good agreement with the observational results.

We also compared observational data with simulated quasars around  $L_*$ , calculated using equation 9 from Hopkins et al. (2007), and selecting objects with an intrinsic luminosity larger than  $L_*/0.5$  dex (which corresponds to a minimum luminosity approximately 1.2 mag fainter than  $M_*$ ). Our predictions for the correlation length and the bias for  $L_*$  objects as a function of redshifts are shown in Figure 11, again together with the available observational data. The discrepancies with Shen et al. (2008) for the correlation length can be due in differences in the calculation of this quantity (as already mentioned, here we do not fix the value of  $\gamma$ ). For the bias, we show also the best fit from Croom et al. (2005) and the prediction of Hopkins et al. (2007). The latter was probably fitted only up to  $z = 3$ , thus explaining the turn-over at redshifts above 3 that seems to not be consistent with the trend shown by the observations. A good approximation to our prediction for the bias is given by the fitting function

$$b(z) = 0.42 + 0.04(1+z) + 0.25(1+z)^2. \quad (14)$$

Quasars with luminosities around  $L_*$  are typically objects very close to their peak luminosity, therefore correspond to objects accreting at high Eddington ratios. As mentioned before, we cannot use these results as a sensitive test of our lightcurve models. However, the good agreement with observations indicates that our merger-triggered BH accretion model predicts a spatial distribution of quasars that is consistent with observations. This is a prediction of a consistent model of the joint evolution of dark matter, galaxies and black holes, evolving  $\Lambda$ CDM initial conditions from high redshift to the present. While the parameters of the semi-analytic model had been tuned to fit the bulk  $z = 0$  properties of the BH population and the AGN luminosity function as a function of redshift, information on clustering had not been considered in the construction of the model, and therefore must be regarded as genuine model predictions.

#### 4 BHS, QUASARS AND THEIR DARK ENVIRONMENT

In this section we explore directly the connection between BHs, quasars and their dark matter environment. As in our simulations the dark matter halo merger trees are the backbone upon which the baryonic component is treated, we can also use them to study the dark environment of our AGN. This in particular allows tests of the validity of the approach typically adopted in the interpretation of observational quasar clustering results (e.g. Porciani et al. 2004; Croom et al. 2005), where the observed quasar bias is compared with the halo bias predicted by analytical halo models (e.g. Mo & White 1996; Sheth & Tormen 1999).

The mass distribution of the haloes hosting AGN of given luminosities,  $P(M_{\text{Halo}}|L_{\text{AGN}})$ , is shown in Figure 12. The AGN are

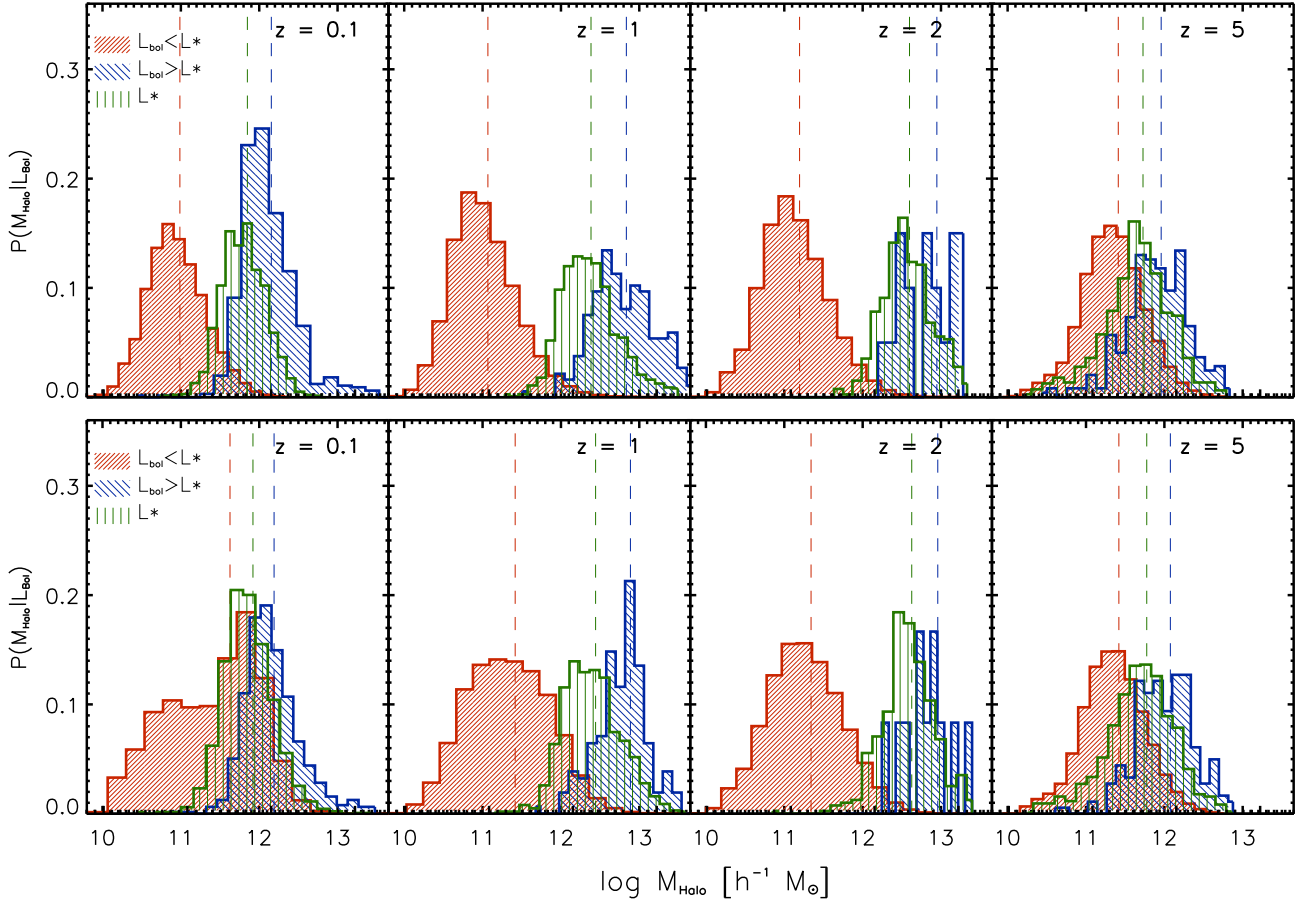


**Figure 12.** Distribution of dark matter halo masses hosting faint-AGN, bright AGN and  $L_*$  quasars. The vertical dashed line indicates the median of the distribution for each luminosity bin, and we refer the reader to the legend on the plot for details in the color/pattern-coding. The AGN have been obtained using Mod I (upper panel) of Mod II (lower panel) for the lightcurve, respectively.

here sub-divided into a faint and a bright sub-sample, depending on their bolometric intrinsic luminosity. The cut in bolometric luminosity is here  $L_*$ , calculated in the same way as for section 3.4. Based on the results on the Eddington ratio distribution (see Figure 4) and on the clustering, we expect the distribution of the masses of the haloes hosting bright AGN to be similar both for Mod I and Mod II. The main difference should be in the distribution of haloes hosting faint AGN: in the Eddington-limited model, the faint AGN population is composed of small-mass BHs accreting at Eddington, whereas in the model that includes a long quiescent phase the faint-AGN population at low redshifts includes also quite massive BHs accreting at low Eddington ratios.

In Figure 12 we indeed see that for Mod I there is a direct proportionality between the luminosity of the AGN and the mass of the host halo: the brighter the AGN, the larger the BH and the host halo. Instead, for Mod II most of the low-luminosity AGN at low redshifts are hosted by more massive haloes, i.e., massive BHs accreting at low Eddington ratio. In the same figures we also plot the mass distribution of haloes hosting  $L_*$  quasars. To get a large enough sample, at any given redshift we included objects in a range of  $\pm 0.5$  dex around  $L_*$ . The similar behavior of haloes hosting  $L_*$  quasars in both models suggests that  $L_*$  objects are mainly BHs accreting close to the Eddington limit.

The mean values of the distributions are shown as a function of redshift in Figure 13. In recent years many groups have analyzed

the clustering properties of quasars to estimate the typical mass of their host haloes, at low- (Padmanabhan et al. 2008), intermediate- (Croom et al. 2005; Porciani et al. 2004; da Ângela et al. 2008; Myers et al. 2007) and high- (Shen et al. 2007) redshifts. These works used quasars observed with SDSS and 2dF, with a typical luminosity around  $L_*$  (except for the very high-redshifts measurements). The masses of the dark matter haloes hosting quasars estimated by these groups are overplotted in Figure 13. Almost all these estimates are in the range predicted by our model: the typical halo mass hosting  $L_*$  quasars seems to grow up to  $z \approx 1.5 - 2$ , and then it decreases again at higher redshifts. To compactly represent our simulation results, we fitted our results with a cubic function

$$M_{\text{halo}} = a_0 + a_1 z + a_2 z^2 + a_3 z^3, \quad (15)$$

with  $a_i = [11.873; 0.944; -0.318; 0.026]$  for the second panel of Figure 13 (the values of these coefficients are similar for the fit of the  $L_*$  curve of the upper panel, which we omit for brevity).

Our results for bright quasars (objects around  $L_*$ ) are also consistent with the estimates of Lidz et al. (2006) and Hopkins et al. (2007), who calculate that the typical mass of haloes hosting quasars is  $\approx 4 \times 10^{12} h^{-1} M_{\odot}$ . These authors argue that bright and faint quasars are the same type of objects but seen in different evolutionary states, and therefore their typical host halo mass should be similar. Since only the brightest quasars are objects accreting at high  $f_{\text{Edd}}$ , only for these objects we expect a tight relation between

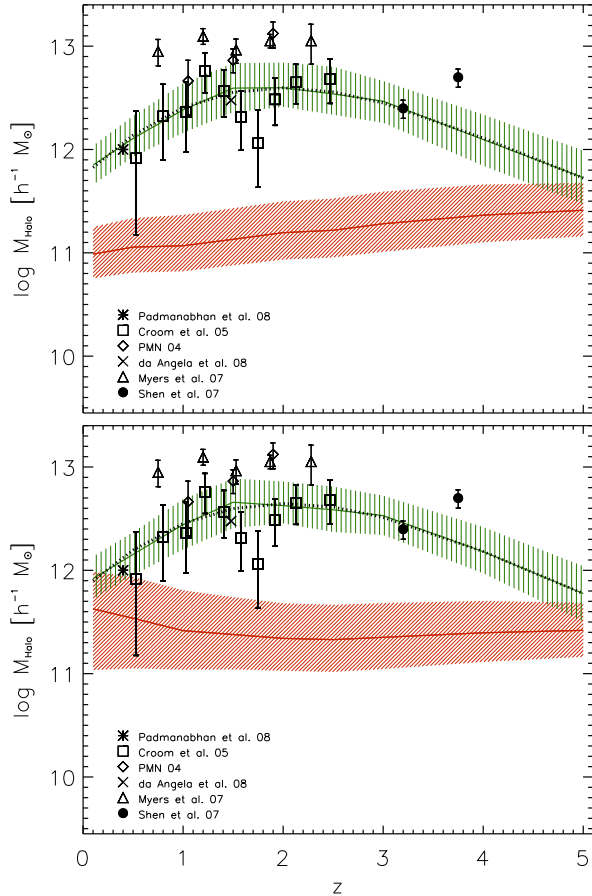


**Figure 13.** In these two panels we show the redshift evolution of the median mass of dark matter haloes hosting AGN of different luminosities from the previous Figure (12). For clarity in the plot, we only show the values obtained for objects with  $L_{\text{Bol}} < L_*$  and with  $L_{\text{Bol}} \sim L_*$ . The dotted black curve shows the best fit to the evolution of the typical host mass of  $L_*$  quasars. The contours indicate the 25 and 75 percentiles. We overplot here estimates obtained by different groups who examined the clustering properties of observed quasars (see legend on the plots).

the instantaneous luminosity and the host halo mass. The relation between AGN luminosity and halo mass is shown in Figure 14. Indeed, only for the very bright quasars there is a direct proportionality between luminosity and halo mass. These are objects that are close to their peak luminosity, have accreted most of the gas available, and at this point their BH is tightly correlated with the mass of the host halo (see also next figure). During the rising phase of the lightcurve (even if BHs are accreting at Eddington), BHs are not yet strongly correlated with the host halo, reflected in a lack of correlation between quasar luminosity and halo mass. During the decaying phase, Mod II produces a dense population of faint objects sitting in massive haloes (see open circles in Figure 14).

White et al. (2008) claimed that the very high bias observed for high-redshift quasars implies a small dispersion in the above relation. Estimates of high Eddington ratios for bright objects at high redshifts (Kollmeier et al. 2006; Shen et al. 2008) indeed seem to support that for very bright objects a tight relation exists between quasar luminosity and halo mass (Fine et al. 2006). However, we would like to point out that just looking at the bright quasar population it is not sufficient to distinguish between different lightcurve models.

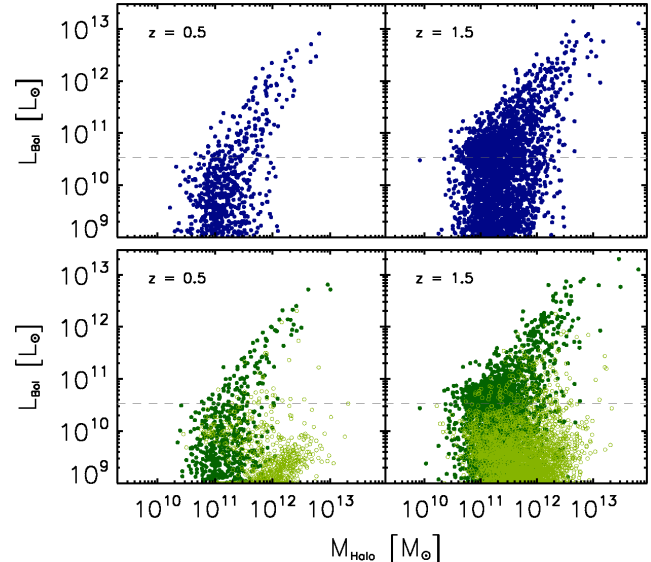


**Figure 14.** Relation of  $L_{\text{Bol}}$  of the AGN versus dark matter halo mass. In the upper panel, BHs accrete according to the Mod I lightcurve, while in the lower panel the predictions are produced using Mod II. While all very bright objects are BHs accreting close to the Eddington limit, the main difference between the two models lies in the faint objects, where we have a dense population of faint AGN hosted by large haloes (the light-green open circles in the lower panel refer to AGN in the quiescent phase). For reference, the dashed line marks the Eddington luminosity corresponding to a BH mass of  $10^6 M_{\odot}$ .

The observed scaling relations between BH masses and different properties of the host galaxy have suggested the possibility of a more fundamental connection between the mass of the BH and the host system. Using measurements of stellar velocity dispersions and assuming a relation between this quantity and the circular velocity of the galaxy and the BH mass, Ferrarese (2002), Baes et al. (2003) and Shankar et al. (2006) estimated how the BH mass could be connected to the dark halo mass in the local universe. At higher redshifts these estimates are of course more problematic, because studies of the stellar kinematics are unavailable and we also are not certain yet how the  $M_{\text{BH}} - \sigma$  relation evolves with redshift. Fine et al. (2006) explored the relation between BHs and quasar host haloes at  $z = 0.5 - 2.5$  using BH virial masses estimates from the width of broad emission lines and DM halo mass obtained from quasar clustering from Croom et al. (2005). In Figure 15, we plot the  $M_{\text{BH}} - M_{\text{Halo}}$  relation for our simulated BHs. We include here only BHs residing in central galaxies of FOF haloes. This is because in our model only central galaxies can merge, and therefore it is mainly BHs hosted by FOF haloes that can grow (the results of Li et al. (2006) indicate that this could be supported by observations). Indeed, we find a well-defined relation which gets tighter with decreasing redshift. In Paper I we already showed this relation at redshift  $z = 0$  and we found good agreement with other works (Ferrarese 2002; Baes et al. 2003; Shankar et al. 2006). Here we overplot the results of Ferrarese (2002) and Shankar et al. (2006) at  $z = 0.1$  for reference; at  $z = 1$  we overplot the zero-point in the relation estimated by Fine et al. (2006) ( $M_{\text{BH}} = 10^{8.4 \pm 0.2} M_{\odot}$  for a halo of  $M_{\text{halo}} = 10^{12.5} M_{\odot}$ ) and at  $z = 1$  and  $z = 2$  the results from direct hydrodynamical simulations of Colberg & di Matteo (2008) (for  $z = 2$  we used their result at  $z = 3$ ).

Note that the fact that BHs need to accrete most of the

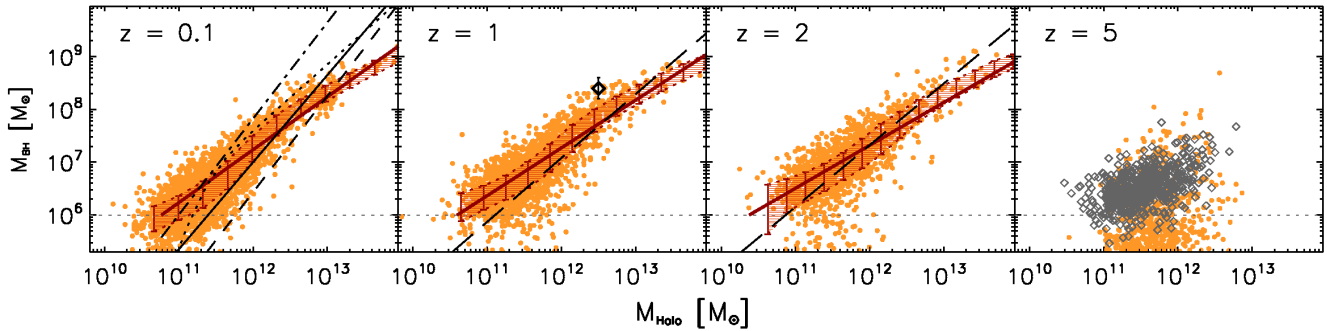


**Figure 15.**  $M_{\text{BH}} - M_{\text{Halo}}$  relation for BHs sitting in central galaxies. The points are our simulated objects, and the red line is the best-fit assuming a linear relation. The filled region encloses the 25 and 75 percentiles. For reference, we show at  $z = 0.1$  the result that Ferrarese (2002) obtained at  $z = 0$  assuming  $v_{\text{vir}} = v_c$  (dashed line),  $v_c = 1.8v_{\text{vir}}$  (dot-dashed line) and the prescription from Bullock et al. (2001) for this relation (solid line). At  $z = 0.1$  we show also the result from Shankar et al. (2006) (dotted curve). The point at  $z = 1$  is the zero-point of this relation obtained by Fine et al. (2006). The dashed lines at  $z = 1$  and at  $z = 2$  are from Colberg & di Matteo (2008) (for  $z = 2$  we used their result at  $z = 3$ ). The horizontal dashed line marks  $M_{\text{BH}} = 10^6 M_{\odot}$ , which is approximately our resolution. This plot was obtained assuming Mod I for the lightcurve, but the result does not change using Mod II, since the final BH masses are the same. The diamonds at  $z = 5$  show the relation between BH mass and halo mass if BHs accreted the available mass instantaneously.

available gas before they ‘sit’ on the above relation could be influenced at high redshifts by the resolution limit of the Millennium simulation, which does not resolve low-mass haloes below  $\sim 10^{10} h^{-1} M_{\odot}$ . We will explore this high-redshift behavior in more details in future work.

#### 4.1 Duty cycle

The time BHs spend shining as quasars is still an open question (see review by Martini 2004). The definition itself of a ‘quasar lifetime’ is somewhat ambiguous. Observationally it is defined as the time BHs spend shining at luminosities higher than some limit (for quasars, the usual definition is the time an active nuclei shines with a B-band magnitude  $M_B < -23$  mag). Theoretically, it can be defined in a simpler way as the total time a BH shines at high Eddington ratio. The quasar lifetime is often also simply defined through the duty cycle, which is given by ratio of the quasar number density and the number density of the haloes that can host them:  $t_q \sim t_{\text{Hubble}} n_q / n_{\text{Halo}}$  (e.g., Adelberger & Steidel 2005).

Haiman & Hui (2001) and Martini & Weinberg (2001) suggested to use the observed quasar clustering to estimate the quasar lifetime, upon the assumption that a monotonic relation exists between quasar luminosity and halo mass (see also Haehnelt et al. 1998). Adelberger & Steidel (2005) pointed out that the theoretical estimate of the duty cycle through clustering analysis depends on the Eddington ratio distribution, on obscuration and on the scatter in the relation between quasar luminosity and halo mass. As we have seen, the assumption of a tight relation between luminosity and halo mass is overly simplistic for realistic lifetime models, and it is therefore interesting to use our simulations directly to examine the distribution of quasar lifetimes.

In Figure 16 we show the fraction of active haloes (or duty cycle), as a function of quasar luminosity, redshift and halo mass, for both Mod I (left panels) and Mod II (right panels). At high redshifts massive haloes have a very high duty cycle, i.e., most of haloes host a bright quasar. As expected, the duty cycle evolves more strongly with redshift for the more luminous AGN: by redshift  $z = 0.1$  only  $\approx 0.1\%$  of the more massive haloes host a quasar, and this result is independent on the lightcurve model assumed. Again, the difference in the two models is in the faint AGN population: the duty cycle of faint objects evolves strongly with redshift and mass for

Mod I, since at low redshift only the smallest haloes host an active BH. On the other side, if the AGN lightcurve includes a long low-level phase, then at low redshift also massive haloes are hosting a low-luminosity object.

Estimates of the quasar lifetime obtained from quasar clustering suggest timescales of the order of  $10^7 - 10^8$  yr, depending on the redshift. At high redshifts ( $z \geq 3.5$ ), Shen et al. (2007) estimated lifetimes of the order of  $30 \sim 600$  Myr, while at  $2.9 \leq z < 3.5$  the estimated range decreases to  $4 \sim 50$  Myr. Porciani et al. (2004) suggest  $t_q \sim 10^7$  yr at  $z \sim 1$ , and values approaching  $10^8$  yr at higher redshifts. As we approach low redshifts and the local universe, the quasar lifetimes seem to decrease: Padmanabhan et al. (2008) suggest values  $< 10^7$  yr for their sample of quasars at  $0.2 < z < 0.6$ . As we have shown in Figure 16, a strong evolution of the quasar lifetime is also expected from our models: at intermediate-high redshifts our results are compatible with lifetimes of a few  $10^8$  yr, but the detailed evolution of the duty cycle also depends strongly on the range of host halo mass considered.

## 5 CONCLUSIONS

In this series of papers we investigate semi-analytic models for BH accretion and quasar emission in the context of a comprehensive galaxy formation model developed for the Millennium Simulation. The physical scenario for BH growth we study is based on the model for BH accretion from Kauffmann & Haehnelt (2000), as revised by Croton et al. (2006), which assumes that galaxy mergers are the primary physical mechanism responsible for efficiently feeding central BHs. In Paper I (Marulli et al. 2008) we used the most recent observations of the local BH population to test basic predictions of the model for the local BH demographics, testing also different theoretical models for the quasar lifetime with goal to reproduce the observed quasar luminosity function. We found an overall good agreement between the predicted and the observed BH properties, and that the faint-end of the observed luminosity function can be better reproduced when a quasar lightcurve model is adopted that includes long quiescent accretion after an Eddington-limited accretion phase.

In the present work we used the spatial distribution of active BHs as a further test of our model for BH accretion. Throughout



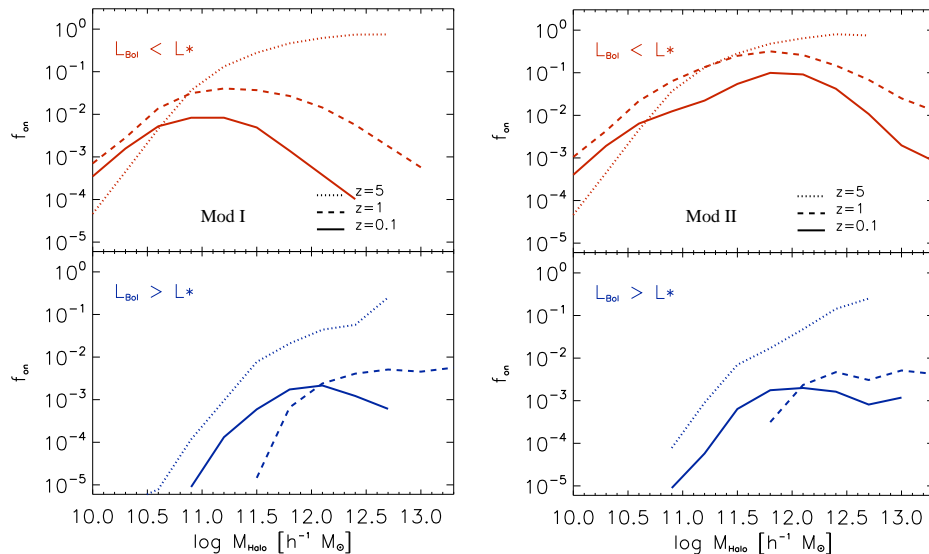


**Figure 16.** Fraction of active haloes (or duty cycle), as a function of redshift, halo mass and AGN luminosity. We compare the results obtained for Mod I (left panels) and Mod II (right panels).

the paper, we compared the results obtained adopting two different theoretical models for the quasar lifetime: pure Eddington-limited accretion (Mod I), and a model in which Eddington-limited accretion is followed by a long, weak accretion phase (Mod II), modeled after Hopkins et al. (2005). The main difference between the predictions of the two models is in the faint-end of the luminosity function. The long low-luminosity accretion phase allowed by Mod II gives rise to a large population of massive BHs that at low redshifts are accreting at low Eddington ratios, in agreement with the observational results of, for example, Heckman et al. (2004) and Netzer & Trakhtenbrot (2007), who found that in the local universe only BHs with mass  $\lesssim 10^7 M_\odot$  are experiencing high-efficient accretion. As also recently pointed out by Hopkins & Hernquist (2008), it is only by studying the properties of the faint AGN population that the quiescent phase described by Hopkins et al. (2005) can be tested.

Independent of the model adopted for the lightcurve, the two-point correlation function of our simulated AGN can be approximated by a single power-law in the range  $0.5 \lesssim r \lesssim 20 h^{-1} \text{Mpc}$ . The bias between AGN and the dark matter is a strong function of redshift, but, at a given epoch, it is approximately constant in the range  $1.0 \lesssim r \lesssim 20 h^{-1} \text{Mpc}$ . As expected, the correlation lengths of AGN obtained with Mod I or Mod II differ only for the faint population: the correlation length of faint AGN obtained with Mod II is consistent with the correlation length of  $10^{12} - 10^{13} h^{-1} M_\odot$  haloes, whereas faint AGN obtained with Mod I exhibit the same clustering as  $10^{11} - 10^{12} h^{-1} M_\odot$  haloes.

Recent results from optical quasar surveys like SDSS and 2dFQSO have not found evidence for a strong dependence of clustering on luminosity (Porciani et al. 2004; Croom et al. 2005; Myers et al. 2007; da Ángela et al. 2008, e.g.), except for Shen et al. (2008) who detect an excess of clustering for their 10% brightest quasars. Our results are consistent with these observations if we consider only quasars with an intrinsic luminosity within the range probed by these surveys. However, if we compare the clustering properties of AGN over a very extended range of luminosity, then the correlation length becomes a moderately strong function of

luminosity and the value of the correlation length of the faint population in particular is seen to depend on the lightcurve model assumed. The fact that the clustering of the observed quasars does not depend on luminosity could be explained in two ways: quasars of different luminosities are powered by BHs of the same mass that are in different stages of their evolution, and/or the typical mass of haloes hosting quasars is approximately constant for the luminosity range probed by observations. From our results the second hypothesis seems to be clearly favoured. The mass range of haloes hosting  $L_*$  quasars is narrow enough that a significant luminosity dependence of clustering cannot be detected with the current observational samples, independent of the lightcurve model.

We also directly compared the clustering of our  $L_*$  quasars with the most recent observational data, and found very good agreement. Since quasars at these luminosities are objects very close to their peak luminosity, and therefore correspond to objects accreting at high Eddington ratios, we cannot, however, use these results as a sensitive test of our lightcurve models. Nevertheless, the good agreement with observations indicates that our merger-triggered BH accretion model predicts a spatial distribution of quasar that is consistent with observations. This non-trivial outcome can be viewed as a further success of the hierarchical galaxy formation paradigm, and the cold dark matter hypothesis.

We note that a similar result for the luminosity dependence of AGN clustering has been found in Marulli et al. (2009), who analyzed mock AGN Chandra catalogues constructed with the same semi-analytic model adopted in this work. Furthermore, Thacker et al. (2009) have recently found very similar results modeling the AGN spatial properties in an hydrodynamical simulation.

In future work we will compare the merger-triggered quasar model with alternative suggestions for the physical triggering mechanism of quasar activity, such as disk-instabilities occurring in isolated galaxies. We expect that quasar clustering statistics can here be a potentially powerful discriminant to further constrain the viable physical models for the evolution of supermassive black holes, and their co-evolution with galaxies.



**ACKNOWLEDGMENTS**

We thank Gabriella De Lucia and Andrea Merloni for many interesting discussions and valuable suggestions. SB acknowledges the PhD fellowship of the International Max Planck Research School in Astrophysics. LM, EB and FM acknowledge partial support by ASI contract I/016/07/0 "COFIS", ASI-INAF I/023/05/0, ASI-INAF I/088/06/0.

**REFERENCES**

- Adelberger K. L., Steidel C. C., 2005, *ApJ*, 630, 50
- Alvarez M. A., Wise J. H., Abel T., 2008, in O’Shea B. W., Heger A., eds, *First Stars III* Vol. 990 of American Institute of Physics Conference Series, Black Hole Remnants of the First Stars. pp 432–434
- Baes M., Buyle P., Hau G. K. T., Dejonghe H., 2003, *MNRAS*, 341, L44
- Bajlik S., Duncan R. C., Ostriker J. P., 1988, *ApJ*, 327, 570
- Barnes J. E., Hernquist L., 1996, *ApJ*, 471, 115
- Best P. N., Kauffmann G., Heckman T. M., Brinchmann J., Charlot S., Ivezić Ž., White S. D. M., 2005, *MNRAS*, 362, 25
- Bromm V., Loeb A., 2003, *ApJ*, 596, 34
- Bullock J. S., Kolatt T. S., Sigad Y., Somerville R. S., Kravtsov A. V., Klypin A. A., Primack J. R., Dekel A., 2001, *MNRAS*, 321, 559
- Carswell R. F., Whelan J. A. J., Smith M. G., Boksenberg A., Tytler D., 1982, *MNRAS*, 198, 91
- Cattaneo A., Bernardi M., 2003, *MNRAS*, 344, 45
- Cattaneo A., Blaizot J., Devriendt J., Guiderdoni B., 2005, *MNRAS*, 364, 407
- Coil A. L., Hennawi J. F., Newman J. A., Cooper M. C., Davis M., 2007, *ApJ*, 654, 115
- Colberg J. M., di Matteo T., 2008, *MNRAS*, 387, 1163
- Cole S., Kaiser N., 1989, *MNRAS*, 237, 1127
- Cowie L. L., Barger A. J., Bautz M. W., Brandt W. N., Garmire G. P., 2003, *ApJ*, 584, L57
- Croom S. M., Boyle B. J., Shanks T., Smith R. J., Miller L., Outram P. J., Loaring N. S., Hoyle F., da Ângela J., 2005, *MNRAS*, 356, 415
- Croom S. M., Smith R. J., Boyle B. J., Shanks T., Miller L., Outram P. J., Loaring N. S., 2004, *MNRAS*, 349, 1397
- Croton D. J., 2006, *MNRAS*, 369, 1808
- Croton D. J., Springel V., White S. D. M., De Lucia G., Frenk C. S., Gao L., Jenkins A., Kauffmann G., et al., 2006, *MNRAS*, 365, 11
- da Ângela J., Shanks T., Croom S. M., Weilbacher P., Brunner R. J., Couch W. J., Miller L., Myers A. D., et al., 2008, *MNRAS*, 383, 565
- De Lucia G., Blaizot J., 2007, *MNRAS*, 375, 2
- Di Matteo T., Springel V., Hernquist L., 2005, *Nat*, 433, 604
- Elvis M., Risaliti G., Zamorani G., 2002, *ApJ*, 565, L75
- Fan X., Narayanan V. K., Lupton R. H., Strauss M. A., Knapp G. R., Becker R. H., White R. L., Pentericci L., Leggett S. K., et al., 2001, *AJ*, 122, 2833
- Fan X., White R. L., Davis M., Becker R. H., Strauss M. A., Haiman Z., Schneider D. P., Gregg M. D., et al., 2000, *AJ*, 120, 1167
- Ferrarese L., 2002, *ApJ*, 578, 90
- Ferrarese L., Ford H., 2005, *Space Science Reviews*, 116, 523
- Ferrarese L., Merritt D., 2000, *ApJ*, 539, L9
- Fine S., Croom S. M., Miller L., Babic A., Moore D., Brewer B., Sharp R. G., Boyle B. J., et al., 2006, *MNRAS*, 373, 613
- Graham A. W., Driver S. P., 2007, *MNRAS*, 380, L15
- Grazian A., Negrello M., Moscardini L., Cristiani S., Haehnelt M. G., Matarrese S., Omizzolo A., Vanzella E., 2004, *AJ*, 127, 592
- Haehnelt M. G., Natarajan P., Rees M. J., 1998, *MNRAS*, 300, 817
- Haiman Z., Hui L., 2001, *ApJ*, 547, 27
- Häring N., Rix H.-W., 2004, *ApJ*, 604, L89
- Hasinger G., Miyaji T., Schmidt M., 2005, *A&A*, 441, 417
- Heckman T. M., Kauffmann G., Brinchmann J., Charlot S., Tremonti C., White S. D. M., 2004, *ApJ*, 613, 109
- Heger A., Woosley S. E., 2002, *ApJ*, 567, 532
- Hopkins P. F., Hernquist L., 2008, arXiv:0809.3789
- Hopkins P. F., Hernquist L., Martini P., Cox T. J., Robertson B., Di Matteo T., Springel V., 2005, *ApJ*, 625, L71
- Hopkins P. F., Lidz A., Hernquist L., Coil A. L., Myers A. D., Cox T. J., Spergel D. N., 2007, *ApJ*, 662, 110
- Hopkins P. F., Richards G. T., Hernquist L., 2007, *ApJ*, 654, 731
- Kauffmann G., Haehnelt M., 2000, *MNRAS*, 311, 576
- Kirkman D., Tytler D., 2008, *MNRAS*, 391, 1457
- Kollmeier J. A., Onken C. A., Kochanek C. S., Gould A., Weinberg D. H., Dietrich M., Cool R., Dey A., et al., 2006, *ApJ*, 648, 128
- Koushiappas S. M., Bullock J. S., Dekel A., 2004, *MNRAS*, 354, 292
- Koushiappas S. M., Zentner A. R., 2006, *ApJ*, 639, 7
- Li C., Kauffmann G., Wang L., White S. D. M., Heckman T. M., Jing Y. P., 2006, *MNRAS*, 373, 457
- Lidz A., Hopkins P. F., Cox T. J., Hernquist L., Robertson B., 2006, *ApJ*, 641, 41
- Loeb A., Rasio F. A., 1994, *ApJ*, 432, 52
- Madau P., Rees M. J., 2001, *ApJ*, 551, L27
- Magorrian J., Tremaine S., Richstone D., Bender R., Bower G., Dressler A., Faber S. M., Gebhardt K., et al., 1998, *AJ*, 115, 2285
- Malbon R. K., Baugh C. M., Frenk C. S., Lacey C. G., 2007, *MNRAS*, 382, 1394
- Marconi A., Hunt L. K., 2003, *ApJ*, 589, L21
- Marconi A., Risaliti G., Gilli R., Hunt L. K., Maiolino R., Salvati M., 2004, *MNRAS*, 351, 169
- Martini P., 2004, in Ho L. C., ed., *Coevolution of Black Holes and Galaxies QSO Lifetimes*. pp 169–+
- Martini P., Weinberg D. H., 2001, *ApJ*, 547, 12
- Marulli F., Bonoli S., Branchini E., Gilli R., Moscardini L., Springel V., 2009, arXiv:0809.3789
- Marulli F., Bonoli S., Branchini E., Moscardini L., Springel V., 2008, *MNRAS*, 385, 1846
- Marulli F., Branchini E., Moscardini L., Volonteri M., 2007, *MNRAS*, 375, 649
- Marulli F., Crociani D., Volonteri M., Branchini E., Moscardini L., 2006, *MNRAS*, 368, 1269
- Merloni A., Heinz S., 2008, *MNRAS*, 388, 1011
- Merloni A., Rudnick G., Di Matteo T., 2004, *MNRAS*, 354, L37
- Mo H. J., White S. D. M., 1996, *MNRAS*, 282, 347
- Monaco P., Fontanot F., Taffoni G., 2007, *MNRAS*, 375, 1189
- Myers A. D., Brunner R. J., Nichol R. C., Richards G. T., Schneider D. P., Bahcall N. A., 2007, *ApJ*, 658, 85
- Netzer H., Trakhtenbrot B., 2007, *ApJ*, 654, 754
- Padmanabhan N., White M., Norberg P., Porciani C., 2008, arXiv:0802.2105

- Peacock J. A., 1999, *Cosmological Physics*. *Cosmological Physics*, by John A. Peacock, pp. 704. ISBN 052141072X. Cambridge, UK: Cambridge University Press, January 1999.
- Porciani C., Magliocchetti M., Norberg P., 2004, *MNRAS*, 355, 1010
- Ricotti M., Ostriker J. P., Gnedin N. Y., 2005, *MNRAS*, 357, 207
- Ripamonti E., Mapelli M., Zaroubi S., 2008, *MNRAS*, 387, 158
- Ross N. P., Shen Y., Strauss M. A., Vanden Berk D. E., Connolly A. J., Richards G. T., Schneider D. P., Weinberg D. H., et al., 2009, *ArXiv:0903.3230*
- Sesana A., Haardt F., Madau P., Volonteri M., 2005, *ApJ*, 623, 23
- Shakura N. I., Sunyaev R. A., 1973, *A&A*, 24, 337
- Shankar F., Lapi A., Salucci P., De Zotti G., Danese L., 2006, *ApJ*, 643, 14
- Shankar F., Salucci P., Granato G. L., De Zotti G., Danese L., 2004, *MNRAS*, 354, 1020
- Shen Y., Greene J. E., Strauss M. A., Richards G. T., Schneider D. P., 2008, *ApJ*, 680, 169
- Shen Y., Strauss M. A., Oguri M., Hennawi J. F., Fan X., Richards G. T., Hall P. B., Gunn J. E., et al., 2007, *AJ*, 133, 2222
- Shen Y., Strauss M. A., Ross N. P., Hall P. B., Lin Y.-T., Richards G. T., Schneider D. P., Weinberg D. H., et al., 2008, *ArXiv:0810.4144*
- Sheth R. K., Tormen G., 1999, *MNRAS*, 308, 119
- Silk J., Rees M. J., 1998, *A&A*, 331, L1
- Soltan A., 1982, *MNRAS*, 200, 115
- Spergel D. N., Verde L., Peiris H. V., Komatsu E., Nolte M. R., Bennett C. L., Halpern M., Hinshaw G., et al., 2003, *ApJS*, 148, 175
- Springel V., Di Matteo T., Hernquist L., 2005, *MNRAS*, 361, 776
- Springel V., White S. D. M., Jenkins A., Frenk C. S., Yoshida N., Gao L., Navarro J., Thacker R., et al., 2005, *Nat*, 435, 629
- Springel V., White S. D. M., Tormen G., Kauffmann G., 2001, *MNRAS*, 328, 726
- Steffen A. T., Barger A. J., Cowie L. L., Mushotzky R. F., Yang Y., 2003, *ApJ*, 596, L23
- Thacker R. J., Scannapieco E., Couchman H. M. P., Richardson M., 2009, *ApJ*, 693, 552
- Tremaine S., Gebhardt K., Bender R., Bower G., Dressler A., Faber S. M., Filippenko A. V., Green R., et al., 2002, *ApJ*, 574, 740
- Ueda Y., Akiyama M., Ohta K., Miyaji T., 2003, *ApJ*, 598, 886
- White M., Martini P., Cohn J. D., 2008, *MNRAS*, 390, 1179
- York D. G., Adelman J., Anderson Jr. J. E., Anderson S. F., Annis J., Bahcall N. A., Bakken J. A., Barkhouser R., et al., 2000, *AJ*, 120, 1579
- Yu Q., Tremaine S., 2002, *MNRAS*, 335, 965